Rudolf Huebener

Electrons in Action : Roads to Modern Computers and Electronics

Supplements : Introduction

The author had written this book to tell about the many fascinating advances during the last century in our understanding of the physical properties of materials, which are highly relevant for modern technology and industry. In particular the role of the individual people and quite often of the scientists and engineers at very young age has been emphasized. It was felt that the readers of the book would welcome if mathematical treatments were kept out and mainly the fundamental concepts were presented.

Since publication of the book in 2005 it became more and more clear that the book could well serve as an introductory text for students of physics, chemistry, and electrical engineering, if a supplementary text would be available containing a more detailed (and mathematical) treatment of the subjects discussed in the book. It is this goal, which motivated publisher and author to provide the following supplements online. We hope that in this way the book will be interesting for an extended readership.

In the same spirit I have added at the end a glossary explaining some specific subjects raised in the book.

The author would like to thank Christoph von Friedeburg, Wiley-VCH Verlag, for motivation and encouragement and Marius Orlowski, Virginia Polytechnic Institute, for many discussions and a critical reading of the supplementary text.

Tübingen, June 2009 Rudolf Huebener

2 Well-ordered Lattice Structures in Crystals

Supplement

In a crystal the locations occupied by the atoms or molecules are described mathematically by the lattice vectors

$$\mathbf{r} = n_1\,\mathbf{a} + n_2\,\mathbf{b} + n_3\,\mathbf{c} \qquad (2.1)$$

Here, n_1 , n_2 , and n_3 represent integer numbers. **a**, **b**, and **c** are three fundamental translation vectors. Here and in the following vectors are denoted by bold symbols. All values of the integers n_1 , n_2 , n_3 yield the lattice points of the crystal. (In (2.1) we assume that the origin of the coordinate system is located at a lattice point). The translation vectors **a**, **b**, **c** generate the elementary cell (Fig. 2.9), which in turn yields the crystal lattice by its spatial repetition. By a special choice of the lengths of the three vectors **a**, **b**, **c** of the elementary cell (lattice constants) and of the three angles between them one finds seven fundamental types of crystal lattices. If additional lattice points at special locations of the elementary cell (middle of the outer surfaces or its center) are added, one can show that a total of only 14 translational lattices can be generated. These are the 14 Bravais lattices shown in Fig. 2.3

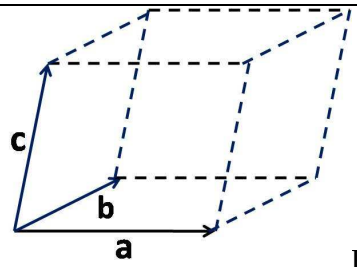

Figure 2.9: Elementary cell generated by the translation vectors **a**, **b**, **c** .

Of course, the structure of crystals is usually more complex than that of one of the 14 Bravais lattices. Here symmetry considerations play a crucial role. The crystal lattice is reproduced exactly following the fundamental symmetry operations: translation, rotation, reflection at a mirror plane, and inversion (at a point). In the case of the rotation operation one distinguishes, how often the crystal lattice is reproduced during a complete rotation by 2π. One- , two- , three- , four- , and six-fold rotation axes are possible, corresponding to rotations by 2π, $2\pi/2$, $2\pi/3$, $2\pi/4$, and $2\pi/6$, respectively. The combination of rotation, reflection at a mirror plane, and inversion specifies one of the 32 point groups. Including also the translation, one obtains one of the 230 space groups characterizing any crystal structure.

The structure of crystals can be clarified using the diffraction of X-rays. It is the similarity of the magnitude of the wavelength of the X-rays and of the distance between the neighboring objects in the crystal (lattice constant), which provides this opportunity by means of interference. In the case of the diffraction of X-rays, at each lattice point of the crystal a spherically propagating electromagnetic wave is generated which interferes with the waves originating at the neighboring lattice points. In the case of two lattice points, the interference pattern is shown schematically in Fig. 2.6, with the maxima and minima of the resulting total wave amplitude depending on the propagation direction.

Looking at this situation in more detail, we consider the (elastic) reflection of the wave at a series of parallel lattice planes. Denoting the distance between neighboring lattice planes a, and the angle between the planes and the direction of the incoming and of the outgoing wave θ (see Fig. 2.10), the difference between the distance covered by the waves reflected at two neighboring planes is $2\,a\sin\theta$. For constructive interference, at which the amplitudes of both waves exactly add to each other, this distance must be equal to an integer multiple of the wavelength λ. This leads to the famous Bragg reflection law

$$2\,a\sin\theta = n\,\lambda \qquad (2.2)$$

where n is an integer.

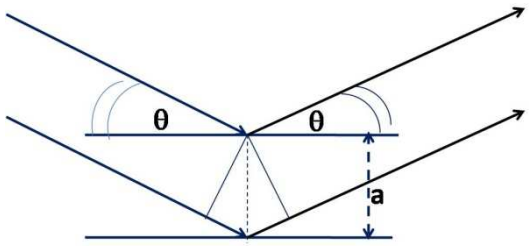

Figure 2.10: The reflection of the wave at two parallel lattice planes separated from each other by the distance a results in the additional distance $2\,a\sin\theta$ covered by the wave reflected at the lower plane. θ is the angle between the planes and the incoming and the outgoing wave.

So far we have considered only a single series of parallel lattice planes, all having the same normal vector (vector oriented perpendicular to the planes). However, in the case of a three-dimensional crystal we deal also with other lattice planes characterized by different normal vectors. In general, the directions of constructive interference for differently oriented lattice planes do not coincide, and a clear maximum diffraction signal at distinct diffraction angles

only appears in the case of special selected values of the wavelength or frequency of the X-rays. This is illustrated schematically in Fig. 2.7 and leads to the famous Laue diffraction diagram, an example of which is shown in Fig. 2.1.

The phenomena associated with the wave propagation in a spatially periodic (crystal) lattice (periodic potential) can be described mathematically in a particularly simple way using the concept of the reciprocal lattice. This concept is based on the abstract mathematical wave-vector space (Fourier space) and had been introduced by the American J. W. Gibbs. A wave propagating along the x-direction can be written as the complex function

$$F(x,t) = F_o\, e^{i(kx-\omega t)} \tag{2.3}$$

Here t is the time and ω the angular frequency. The wave number k is related to the wavelength λ through the relation $k = 2\pi / \lambda$. In the case of three dimensions the function (2.3) can be generalized yielding

$$F(\mathbf{r},t) = F_o\, e^{i(\mathbf{k}\,\mathbf{r}-\omega t)} \tag{2.4}$$

where $\mathbf{r} = \mathbf{x} + \mathbf{y} + \mathbf{z}$ and $\mathbf{k} = \mathbf{k_x} + \mathbf{k}_y + \mathbf{k}_z$. The wave number k of the one-dimensional case is replaced by the wave vector **k** having the three components $\mathbf{k_x}$, $\mathbf{k}_y$, $\mathbf{k}_z$.

The reciprocal lattice **G** is defined in the following way

$$\mathbf{G} = h_1\,\mathbf{A} + h_2\,\mathbf{B} + h_3\,\mathbf{C} \tag{2.5}$$

where h_1 , h_2 , h_3 represent integer numbers. The fundamental vectors **A** , **B** , **C** are connected with the translational vectors **a** , **b** , **c** of the elementary cell (see Fig. 2.9). They are defined as follows

$$\mathbf{A} = 2\pi\,\frac{\mathbf{b}\times\mathbf{c}}{\mathbf{a}\,\mathbf{b}\times\mathbf{c}}\,; \quad \mathbf{B} = 2\pi\,\frac{\mathbf{c}\times\mathbf{a}}{\mathbf{a}\,\mathbf{b}\times\mathbf{c}}\,; \quad \mathbf{C} = 2\pi\,\frac{\mathbf{a}\times\mathbf{b}}{\mathbf{a}\,\mathbf{b}\times\mathbf{c}} \tag{2.6}$$

We see that **A** , **B** , **C** of the reciprocal lattice are oriented perpendicular to two fundamental axes of the crystal lattice, respectively.

It can be shown that a function U(**r**), reproducing exactly the periodicity of the crystal lattice, is obtained in the form

$$U(\mathbf{r}) = \sum_{\mathbf{G}} u_{\mathbf{G}}\, e^{i\,\mathbf{G}\,\mathbf{r}} \tag{2.7}$$

This function satisfies the periodicity condition

$$U(\mathbf{r} + \boldsymbol{\rho}) = U(\mathbf{r}) , \tag{2.8}$$

where $\boldsymbol{\rho}$ is a lattice vector of the form given in (2.1). Furthermore, the Bragg condition for the constructive interference between two waves scattered by the crystal from the incoming wave vector **k** into the outgoing wave vector **k´** can simply be written as

$$\mathbf{k´} - \mathbf{k} = \mathbf{G} \tag{2.9}$$

The simplicity of Eqs. (2.7) and (2.9) illustrates the advantage achieved by using the concept of the reciprocal lattice.

The abstract wave-vector space (**k**-space) with the reciprocal lattice is divided into the Brillouin zones. The boundaries of the Brillouin zones are obtained from the planes passing perpendicularly through a reciprocal-lattice vector at half of its value. Including larger and larger reciprocal-lattice vectors in this construction, the first, second, third, etc. Brillouin zones are found. In Fig. 2.11 we show the first Brillouin zone in the (two-dimensional) case of the two fundamental vectors **A** and **B** oriented perpendicular to each other. As we will see in Chapter 4, the Brillouin zones play an important role for the electronic band structure of materials.

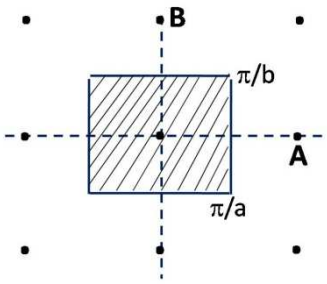

Figure 2.11: Construction of the first Brillouin zone in the (two-dimensional) case of the two fundamental reciprocal lattice vectors **A** and **B** oriented perpendicular to each other.

3 Permanent Movement in the Crystal Lattice

Supplement

The quantization of the vibrational energy of the atoms or molecules in a crystal is clearly demonstrated by the temperature dependence of the specific heat. According to the Einstein model, the crystal energy U contained in the lattice vibrations is

$$U = 3\,N < n_\omega > \hbar\omega \tag{3.1}$$

Here we assume a crystal consisting of N atoms. Hence, there exist 3N degrees of freedom of the vibrations. $< n_\omega >$ is the probability of a vibrational state with the angular frequency ω and the quantized energy $\hbar\omega$ being occupied. This probability is given by the Bose-Einstein distribution

$$< n_\omega > = \frac{1}{e^{\hbar\omega/k_B T} - 1} \tag{3.2}$$

This energy distribution had been proposed for the first time in the form of Planck's famous radiation law in the case of electromagnetic radiation. The quantity $\hbar = h/2\pi$ is Planck's constant h divided by 2π. k_B is Boltzmann's constant, and T is the temperature. In his model Einstein had assumed only a single vibration frequency $\omega = \omega_E$ to appear in Eqs. (3.1) and (3.2).

In the more accurate Debye model, instead of the single Einstein frequency ω_E a continuous frequency spectrum of the vibrations of the crystal lattice is taken into account ranging between zero and a maximum frequency ω_D referred to as Debye frequency. Now the vibrational crystal energy is written as an integral over all phonon frequencies

$$U = \int_0^{\omega_D} d\omega\, D(\omega) < n_\omega > \hbar\omega \tag{3.3}$$

Here $D(\omega)$ is the number of vibrations per frequency interval, also referred to as the density of states. As an example, the spectral energy density of the phonons in a germanium crystal is shown in Fig. 3.4.

The density of states $D(\omega)$ is found by considering the number of elastic eigenmodes fitting exactly into the volume of the crystal, say, into a cube with the length L on each side. In

addition, the increment of the volume in **K**-space with the frequency change $d\omega$ must be taken into account. (We denote the phonon wave vectors by **K**). In this way one finds $D(\omega) \sim \omega^2$. Finally, inserting $< n_\omega >$ from (3.2) into (3.3) the vibration energy of the crystal is obtained. The specific heat (at constant volume) associated with the lattice vibrations then turns out to be

$$C_V = \left(\frac{\partial U}{\partial T}\right)_V = 9\, N\, k_B \left(\frac{T}{\theta}\right)^3 \int_0^{z_D} dz\, \frac{z^4\, e^z}{(e^z-1)^2} \qquad (3.4)$$

Here $\theta = \hbar\omega_D/k_B$ is the Debye temperature. The quantity $z = \hbar\omega/k_BT$ is introduced for convenience. ($z_D = \hbar\omega_D/k_BT = \theta/T$). At low temperatures ($T << \theta$) the expression in (3.4) yields the T^3 dependence of c_V in excellent agreement with the experimental observations. On the other hand, at high temperatures ($T >> \theta$) Eq. (3.4) yields c_V = const, and the classic law of Du Long and Petit is reproduced again.

The thermal conductivity κ_G associated with the lattice vibrations in a crystal is intimately connected with the specific heat of the phonons. This can be seen from the simple formula for the lattice component κ_G of the thermal conductivity obtained from kinetic theory

$$\kappa_G = \frac{1}{3}\, v\, C\, \ell \qquad (3.5)$$

Here v and ℓ are the velocity and mean free path of the phonons, respectively. C is the phonon specific heat per volume. At very low temperatures the phonon mean free path ℓ is limited by phonon scattering at the crystal surfaces, and ℓ becomes temperature independent. In this regime we have $C \sim T^3$ and, hence, from (3.5) $\kappa_G \sim T^3$.

At higher temperatures an important process for the scattering of phonons is the Umklapp process (U-process) due to Peierls. As a result of this process phonon momentum is transferred back to the crystal. Denoting the phonon wave vectors participating in this process by $\mathbf{K}_i$, in the case of a U-process we have

$$\mathbf{K}_1 + \mathbf{K}_2 = \mathbf{K}_3 \pm \mathbf{G} \qquad (3.6)$$

G is a reciprocal lattice vector. Processes with **G** = 0 are referred to as N-processes. (In the previous Chapter in the case of Eq. (2.9) we dealt already with a similar situation, where photon momentum was exchanged with the crystal lattice during Bragg reflection). U-processes become appreciable only when $\mathbf{K}_1 + \mathbf{K}_2 \geq \frac{1}{2}\mathbf{G}$. However, at low temperatures phonons satisfying this condition are not thermally excited, and U-processes are frozen out. At high temperatures ($T > \theta$) U-processes dominate. Their number is proportional to the number of phonons, which in turn is proportional to the temperature. Hence, for the phonon mean free path ℓ we have $\ell \sim T^{-1}$. Since C is constant in this regime, from (3.5) we find $\kappa_G \sim T^{-1}$.

We see that as a function of temperature the lattice thermal conductivity displays a distinct maximum. This is shown schematically in Fig. 3.6.

The variations of the phonon frequency ω with the phonon wave vector **K** is found from a theoretical model, in which the crystal lattice is described in terms of point-like masses occupying the lattice sites and connected with each other by means of elastic springs. In the simplest case of a linear chain with the lattice constant a, consisting of the same masses m connected with the same spring constant f , one obtains the dispersion relation

$$\omega = \left(\frac{4f}{m}\right)^{1/2} \sin\frac{Ka}{2} \qquad (3.7)$$

Since we deal with a discrete lattice with the distance a between its neighbors, the components of the wave vector **K** are limited within the range of the first Brillouin zone, i. e., in the case of the one-dimensional chain to the range $-\frac{\pi}{a} \leq K \leq \frac{\pi}{a}$. In the limit of small wave vectors one obtains from (3.7)

$$\omega = \left(\frac{a^2 f}{m}\right)^{1/2} K \qquad (3.8)$$

The factor $\left(\frac{a^2 \mathrm{f}}{\mathrm{m}}\right)^{1/2}$ represents the sound velocity. Equation (3.8) indicates the acoustic limit, and (3.7) is referred to as an acoustic mode. The three acoustic modes (one longitudinal mode and two transverse modes) observed in a copper crystal along a specific direction is shown in Fig. 3.5. (Because of the face-centered cubic symmetry of copper, the location of the boundary of the first Brillouin zone differs from that of a linear chain or of a simple cubic crystal with the lattice constant a).

Because of the anisotropy of the elastic properties in a crystal, the ballistic propagation of phonon energy shows a preference along distinct crystallographic directions. This effect is referred to as phonon focusing and can be nicely demonstrated by scanning over one crystal surface with a laser or electron beam. The phonons generated in this way at the location irradiated by the beam are detected using a small phonon detector attached to the opposite crystal surface. The principle of this technique is explained in Fig. 3.7, and a typical result is presented in Fig. 3.1.

4 Electrical Conductor or Insulator

Supplement

The quantum mechanical theory of the electrons in a crystal requires the solution of the Schrödinger Equation in the case of the periodic crystal lattice. Here the energy spectrum of the electrons is determined by the periodic potential U(**r**) due to the crystal atoms. The Schrödinger Equation is

$$- \frac{\hbar^2}{2m} \Delta\psi(\mathbf{r}) + U(\mathbf{r})\,\psi(\mathbf{r}) = \varepsilon\,\psi(\mathbf{r}) \qquad (4.1)$$

Here m and $\psi(\mathbf{r})$ are the mass and the wave function of the electrons, respectively. Δ denotes the Laplace operator

$\Delta\psi = \frac{\partial^2\psi}{\partial x^2} + \frac{\partial^2\psi}{\partial y^2} + \frac{\partial^2\psi}{\partial z^2}$ and ε the electron energy. The potential energy U(**r**) must satisfy the periodicity condition (2.8).

In the theoretical treatment two important cases of approximations are distinguished: the bound-electron approximation (due to F. Bloch) and the free-electron approximation (due to R. E. Peierls). In both cases we are concerned only with the electrons residing at the highest available energy levels, and not with the lower bound states in the individual atoms occupying the lattice sites of the crystal.

In the *bound-electron approximation* the electrons with the highest energy are assumed to spend most of the time at a certain lattice atom, experiencing only an occasional transfer to a neighboring lattice site because of the small interaction between these sites. Their binding energy at their specific lattice sites is assumed to be much larger than their kinetic energy. In this case the solution found by Bloch is based on the atomic wave function $\varphi_O(\mathbf{r})$ of a bound electron within a (single) free atom. Denoting the electron coordinate by **r** and the coordinate of the atom (i. e., of the lattice site) by **ρ** , as his solution Bloch proposed the superposition of the atomic wave functions $\varphi_O(\mathbf{r} - \boldsymbol{\rho})$:

$$\psi_k(\mathbf{r}) = \sum_{\boldsymbol{\rho}} e^{i\mathbf{k}\boldsymbol{\rho}}\ \varphi_O(\mathbf{r} - \boldsymbol{\rho}) \qquad (4.2)$$

This ansatz automatically yields the extended periodicity condition

$$\psi_k(\mathbf{r} + \boldsymbol{\rho}) = e^{i\mathbf{k}\boldsymbol{\rho}}\ \psi_k(\mathbf{r}) \qquad (4.3)$$

introducing the phase factor $e^{i\mathbf{k\rho}}$.

With the wave function (4.2) the electron energy ε_k is found to be

$$\varepsilon_k = \varepsilon_O - \alpha - 2\beta(\cos k_x a + \cos k_y a + \cos k_z a) \qquad (4.4)$$

Here ε_O is the electron energy of the unperturbed individual single atom. The correction α is

$$-\alpha = \int d\tau\ \varphi_O^*(\mathbf{r})\,[U(\mathbf{r}) - U_a(\mathbf{r})]\,\varphi_O(\mathbf{r}) \qquad (4.5)$$

$U_a(\mathbf{r})$ is the potential energy of the unperturbed individual atom. As seen in Fig. 4.5, due to the presence of the atoms at the neighboring lattice sites we have $U_a(\mathbf{r}) > U(\mathbf{r})$ and, hence, $\alpha > 0$. So α represents an energy correction arising from the neighboring atoms. The second correction in (4.4) is obtained by assuming for simplicity cubic symmetry of the lattice, and by combining the contributions of the nearest neighbors at the distances $\pm$ a in x, y, and z-direction. The quantity β contains the interaction between the nearest neighbors and is given by

$$-\beta = \int d\tau\ \varphi_O^*(\mathbf{r}-\mathbf{a})\,[U(\mathbf{r}) - U_a(\mathbf{r}])\,\varphi_O(\mathbf{r}) \qquad (4.6)$$

Again, we note that in general $\beta > 0$.

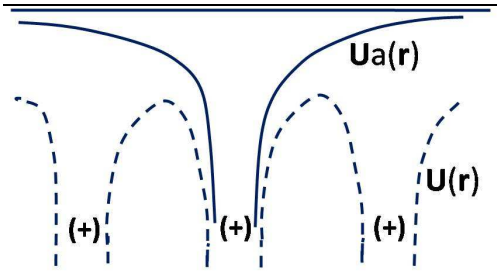

Figure 4.5: Comparison of the potential energy of an electron in the case of a single individual atom, $U_a(\mathbf{r})$ (solid curve), and in the presence of atoms at the neighboring lattice sites, $U(\mathbf{r})$ (dashed curve).

From (4.4) we see that the lowest value of the energy is $\varepsilon = \varepsilon_O - \alpha - 6\beta$. From the highest value $\varepsilon = \varepsilon_O - \alpha + 6\beta$ we note that the width $\Delta\varepsilon$ of the energy band is $\Delta\varepsilon = 12\,\beta$. Because of the increasing overlap between $\varphi_O^*(\mathbf{r}-\mathbf{a})$ and $\varphi_O(\mathbf{r})$ with decreasing lattice

constant a , the quantity β and, hence, the band width $\Delta\varepsilon$ increases. This behavior is shown schematically in Fig. 4.3 in the case of a one-dimensional chain.

So far, we have considered only the interaction of an atom at a specific lattice site with its nearest neighbors. In order to increase the accuracy of the approximation, the interaction with the next-nearest neighbors (and perhaps beyond) may have to be included.

Concluding our discussion of the bound-electron approximation, we see that the interaction with the neighboring lattice atoms leads to a splitting of the energy levels of an individual single atom into energy bands, the energy width of which increases with decreasing distance between the nearest neighbors.

Turning next to the *free-electron approximation*, now we assume that the binding energy of the electrons to a lattice atom is much smaller than their kinetic energy. Neglecting the potential energy U(**r**) in the Schrödinger Equation (4.1), its solution yields the wave function of free electrons

$$\psi(\mathbf{r}) = e^{i\mathbf{kr}} \tag{4.7}$$

with the electron energy

$$\varepsilon = \hbar^2 k^2 / 2m \tag{4.8}$$

The wave function (4.7) represents a planar wave with the wave vector **k** . However, the presence of a very small periodic potential U(**r**) in Eq. (4.1) becomes highly important, if the wave vector **k** is close to the boundary of a Brillouin zone. At the boundary of a Brillouin zone the wave vector **k** exactly satisfies the Bragg condition (2.9), and the wave experiences Bragg reflection. Taking as an example $\mathbf{k} = \mathbf{G_1}/2$, the wave vector changes from **k** to $\mathbf{k}' = \mathbf{k} - \mathbf{G_1} = -\mathbf{G_1}/2$ due to Bragg reflection. This is illustrated schematically in Fig. 4.6 .

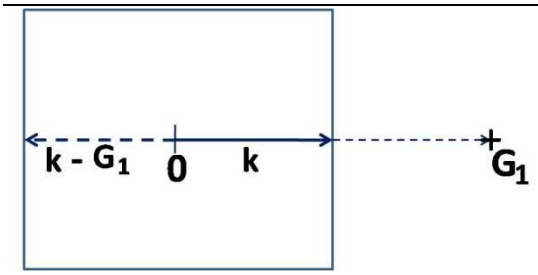

Figure 4.6: Bragg reflection from $\mathbf{k} = \mathbf{G_1}/2$ to $\mathbf{k}' = \mathbf{k} - \mathbf{G_1} = -\mathbf{G_1}/2$.

The solution of the Schrödinger Equation with the periodic potential $U(\mathbf{r})$ can be written as a superposition of plane waves

$$\psi(\mathbf{r}) = \sum_{\mathbf{k}} c_{\mathbf{k}} e^{i\mathbf{kr}} \tag{4.9}$$

Furthermore, expressing the small periodic potential $U(\mathbf{r})$ of the crystal lattice in the form given by Eq. (2.7), in the case $\mathbf{k} = \mathbf{G_1}/2$ one obtains the electron energy

$$\varepsilon = \varepsilon_{\mathbf{k}} \pm u_{\mathbf{G}_1} \tag{4.10}$$

Between the energies $\varepsilon_{\mathbf{k}} + u_{\mathbf{G}_1}$ and $\varepsilon_{\mathbf{k}} - u_{\mathbf{G}_1}$ there appears a forbidden energy gap, in which the propagating-wave solution (4.9) does not exist. The spectral energy curve $\varepsilon(\mathbf{k})$ always approaches the Brillouin-zone boundaries with zero slope. The width of the forbidden energy gap increases with increasing expansion coefficient $u_{\mathbf{G}_1}$, i. e., with increasing potential energy $U(\mathbf{r})$ of the crystal lattice. The appearance of the forbidden energy gaps due to Bragg reflection at the periodic potential of the crystal and a comparison with the case of perfectly free electrons is shown in Fig. 4.2 .

The energy bands occupied by the electrons in a crystal and separated from each other by the forbidden energy gaps immediately provide the answer to the question whether a material is an electrical conductor, insulator, or semiconductor, as first pointed out by A. H. Wilson. Here the crucial argument relies on the fact that preferential motion of the electrons along a specific direction (of an applied electric field) is only possible, if the states of the electronic energy spectrum relevant under the nonequilibrium can become occupied. The result depends critically on the extent to which the upper energy bands are filled up with electrons, and the principle is explained in Fig. 4.4.

5 Metals Obey the Rules of Quantum Statistics

Supplement

We start by discussing the classical models developed mainly by P. Drude and H. A. Lorentz. In an electric field **E** the electrons in a crystal experience the force

$$\mathbf{F} = \hbar \frac{d\mathbf{k}}{dt} = - e \mathbf{E} \tag{5.1}$$

Here **k** denotes the wave vector of the electrons, and e the elementary charge. ($\hbar\mathbf{k}$ is the mechanical momentum of the electrons). According to (5.1), after the time Δt the wave vector increases by the amount $\Delta\mathbf{k}$. In the absence of any scattering processes this increase $\Delta\mathbf{k}$ would become larger and larger. However, scattering of the electrons always occurs (due to phonons or lattice imperfections), resulting in a limited time in which Eq. (5.1) is valid. This limited time is the average time τ between collisions, and we have

$$\hbar \Delta\mathbf{k} = \mathbf{F} \tau = m \Delta\mathbf{v} \tag{5.2}$$

where m and $\Delta\mathbf{v}$ are the electron mass and the drift velocity, respectively. Together with (5.1), the resulting electric current density **j** is

$$\mathbf{j} = n (-e) \Delta\mathbf{v} = n e^2 \frac{\tau}{m} \mathbf{E} \tag{5.3}$$

where n is the electron density. With the electric conductivity σ from the relation $\mathbf{j} = \sigma \mathbf{E}$, we obtain

$$\sigma = n e^2 \tau / m \tag{5.4}$$

We have found Ohm's law, based on the assumption of an average relaxation time τ , which is independent of the electric field **E** .

Since in addition to their electric charge, electrons transport heat energy, they also contribute to the heat conductivity of electric conductors. Hence, the electric conductivity and the electronic part of the heat conductivity are proportional to each other, as can be shown in the following way. In a temperature gradient dT/dx there exists a net energy-current density w from the hot to the cold side given by

$$w = (½)\, n\, v\, \{\varepsilon(T[x - v\,\tau]) - \varepsilon(T[x + v\,\tau])\} \qquad (5.5\ a)$$

$$w = n\, v^2\, \tau \frac{d\varepsilon}{dT} \left(-\frac{dT}{dx}\right) \qquad (5.5\ b)$$

with ε denoting the particle energy. The idea of (5.5) is illustrated in Fig. 5.6.

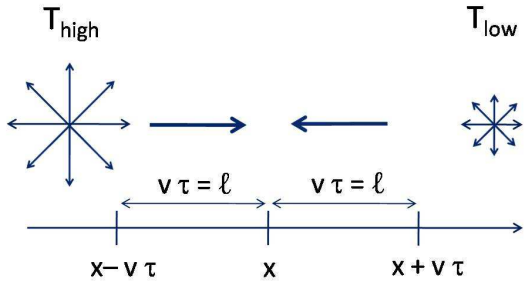

Fig. 5.6: Explanation of the origin of (5.5) describing the heat flux. The arrows at T_{high} and T_{low} indicate the average electron energy.

The electron mean free path $\ell = v\,\tau$ represents the relevant length scale over which the average motion of the electrons up or down the temperature gradient is affected. Using the equipartition theorem

$$\varepsilon = \frac{1}{2} m\, v^2 = \frac{3}{2} k_B\, T \qquad (5.6)$$

and with

$$\frac{d\varepsilon}{dT} = c_V = \frac{3}{2} k_B \qquad (5.7)$$

we obtain the energy-current density

$$w = -\, n \left(\frac{3}{2} k_B\right)^2 \frac{\tau\, T}{m} \frac{dT}{dx} = -\, \kappa_e \frac{dT}{dx} \qquad (5.8)$$

Here we have introduced the thermal conductivity κ_e of the electrons. Together with (5.4) we find

$$L \equiv \frac{\kappa_e}{\sigma\, T} = \frac{9}{4} (k_B/e)^2 \qquad (5.9)$$

The ratio L is referred to as the Lorenz number (named after Ludwig Lorenz). (A more accurate averaging procedure leads to the prefactor $\pi^2/3$ instead of 9/4). The result expressed in (5.9) is the famous Wiedemann-Franz law.

At this stage we have to deal with an important concept introduced by quantum mechanics, namely the fact that the elementary particles such as electrons are exactly identical and cannot be distinguished from each other. The resulting quantum statistics strongly deviates from the classical (Maxwell-Boltzmann) statistics, as we have discussed already in Chapter 3 in the case of the Bose-Einstein distribution (3.2) applying to elementary particles with zero or integer angular momentum and valid for phonons and photons. In the case of electrons we deal with elementary particles having half-integer angular momentum and following the Fermi-Dirac statistics. An important consequence is that fermions must obey the Pauli exclusion principle.

The Fermi-Dirac distribution function is

$$f(\varepsilon) = \frac{1}{e^{(\varepsilon-\varepsilon_F)/k_BT} + 1} \tag{5.10}$$

where ε is the particle energy and ε_F the Fermi energy or chemical potential. This function is shown schematically in Fig. 5.2. At $T = 0$ and $\varepsilon = \varepsilon_F$ the function $f(\varepsilon)$ drops abruptly from the value of 1 to zero, whereas at $T > 0$ this drop spreads over the energy interval of about k_BT .

The Fermi-Dirac distribution of the electrons in a crystal leads to the important result that a large portion of the electrons is “frozen in” energetically and cannot participate in many physical processes. Only the electrons in the energy range of about k_BT near ε_F remain unaffected by this. This effective reduction of the number of the relevant electrons is particularly strong in the case in which $k_BT << \varepsilon_F$. The resulting reduction factor k_BT / ε_F shows up immediately in the electronic component of the specific heat, representing a striking demonstration of the role of quantum statistics. Because of this factor, the specific heat of the electrons is strongly reduced below the value expected from the classical theory. Furthermore, it becomes proportional to the absolute temperature.

Recalling Eq. (4.8) for the electron energy and Figs. 4.2 and 4.3 for the electronic energy-band structure, we note that the electron wave vector **k** represents an important physical quantity. At this point it is advantageous to move the discussion into **k**-space introduced at the end of Supplement 2. The energy states are occupied by electrons up to the Fermi energy ε_F or up to the Fermi wave vector $\mathbf{k}_F = \frac{1}{\hbar} (2\, m\, \varepsilon_F)^{1/2}$ (see Fig. 5.6). In general, in 3-dimensional **k**-space the points at the end of the Fermi wave vectors $\mathbf{k}_F$ constitute a (mostly anisotropic)

surface referred to as the Fermi surface. An example is shown in Fig. 5.1. The Fermi surface represents one of the most important concepts of the physics of electrical conductors.

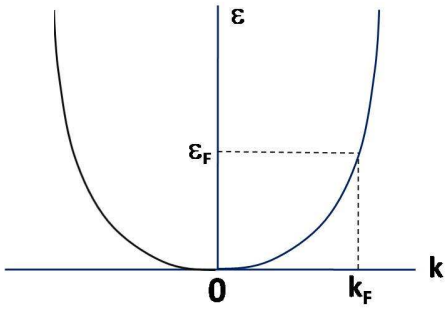

Figure 5.7: The energy spectrum $\varepsilon(\mathbf{k})$ of the electrons is occupied up to the Fermi energy ε_F and to the Fermi wave vector $\mathbf{k}_F$. (It is assumed that $k_BT << \varepsilon_F$).

From Eq. (5.4) for the electric conductivity σ we note that the electric resistivity $\rho = 1/\sigma$ is proportional to the scattering rate τ^{-1} , which determines the temperature dependence of ρ . Starting our discussion with pure metals, the electrons are scattered predominantly by phonons. At temperatures larger than the Debye temperature θ ($T >> \theta$) all phonon states are occupied up to the Debye frequency ω_D , and the number of phonons per state is proportional to T. The latter can be seen from the distribution (3.2). Hence, in this regime one expects $\rho \sim T$. On the other hand, at temperatures much below the Debye temperature θ ($T<<\theta$) the number of the occupied phonon states (contributing to the scattering rate τ^{-1}) increases proportional to T^3 , as we have seen before in the context of Eq. (3.4). Another factor proportional to T^2 arises because of the temperature dependent magnitude of the scattering angle. Altogether one finds $\rho \sim T^5$ in this regime. This behavior represents the famous Bloch-Grüneisen law of the electrical resistance. Its validity is shown in Fig. 5.3.

Electron scattering by crystal imperfections is another important contribution to the electric resistivity. It becomes dominant at very low temperatures where the number of phonons is negligibly small. In good approximation the sacttering rates $1/\tau_i$ associated with the different scattering mechanisms simply add to each other:

$$\frac{1}{\tau} = \sum_i \frac{1}{\tau_i} \qquad (5.11)$$

This fact is referred to as Mathiessen's rule.

Finally, we turn to the thermoelectric effects. The Peltier effect is caused by the fact that an electric current always transports the heat energy of the moving charge carriers in addition to their electric charge (see Fig. 5.4 a). The Peltier coefficient Π is defined as follows

$$\Pi \equiv \frac{\text{heat current density } w_x}{\text{electric current density } j_x} \tag{5.12}$$

At the location of the contact between two conductors A and B the amount of the Peltier heat delivered or taken away per cross-sectional area and time is $(\Pi_A - \Pi_B)\, j_x$, leading to heating or cooling depending on the electric current direction.

In the case of the Seebeck effect we deal with the thermal diffusion of the charge carriers of an electric conductor in a temperature gradient dT/dx (see Fig. 5.4 b). Thermal diffusion is caused by the thermal force $- S_{tr}\, dT/dx$ acting on the particles, where S_{tr} is the transport entropy per particle. As a result, electric charges of opposite sign accumulate at both ends of the conductor, and an electric field E_x is generated. Under equilibrium the thermal force is balanced by the electrostatic force $- e\, E_x$ (taking – e for the charges), and we have the force equation

$$- \quad S_{tr} \frac{dT}{dx} = - e\, E_x = e \frac{dU}{dx} \tag{5.13}$$

where U is the electric potential. We find the Seebeck coefficient (thermoelectric power)

$$S \equiv \frac{\Delta U}{\Delta T} = - \frac{S_{tr}}{e} \tag{5.14}$$

Two conductors A and B soldered together at one end form a thermocouple, which can be highly useful as a thermometer. The temperature difference ΔT between its two ends is found from the potential difference ΔU according to $\Delta U = (S_A - S_B)\, \Delta T$.

Detailed expressions for the thermoelectric coefficients are obtained from transport theory. Here we do not pursue this any further, except to say that in metals the coefficients are sensitively affected by the reduction factor $k_B T/\varepsilon_F$, similarly as the electronic specific heat.

The Peltier coefficient Π and the Seebeck coefficient S of a material are connected with each other through the Thomson relation

$$\Pi = T\, S \tag{5.15}$$

Relation (5.15) represents an example of the reciprocity scheme of the transport coefficients derived by L. Onsager.

6 Less Can Be More: Semiconductors

Supplement

As we have discussed in Chapter 4 and have illustrated in Fig. 4.4 , it is the occupancy of the states within the energy bands, which determines the type of an electric conductor. If there exists an empty band energetically separated from a lower completely filled band by a sufficiently small energy gap, then charge carriers are thermally excited into the empty band, where they can transport an electric current. We deal with a semiconductor. In this case the thermal energy k_BT of the charge carriers represents the key energy. In a semiconductor the concentration of the charge carriers and, hence, the electric conductivity is much smaller than in a metal.

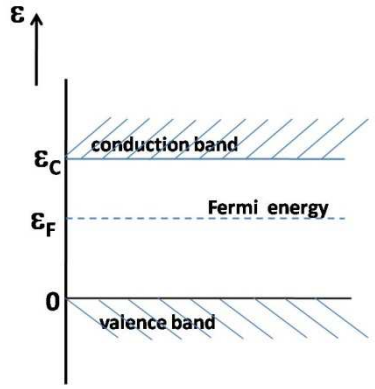

Figure 6.11: Position of valence band and conduction band along the energy axis for an undoped (intrinsic) semiconductor.

In the case of the electrons thermally excited from the valence band into the conduction band we have $\varepsilon - \varepsilon_F >> k_BT$, and the Fermi-Dirac distribution (5.10) can be replaced by the Boltzmann distribution

$$f(\varepsilon) = e^{-(\varepsilon - \varepsilon_F)/\, k_BT} \tag{6.1}$$

Using the energy scale indicated in Fig. 6.11 , the electron concentration in the conduction band per volume turns out to be

$$n = 2\,(2\pi\, m_e\, k_B\, T/\, h^2)^{3/2}\, e^{-(\varepsilon_C - \varepsilon_F)/\, k_BT} \tag{6.2}$$

m_e is the electron mass. We note that the electrons transferred into the conduction band are missing in the valence band, where they represent holes having the distribution $f_h(\varepsilon) = 1 - f(\varepsilon)$. The hole concentration in the valence band per volume is

$$p = 2\,(2\pi\, m_h\, k_B\, T/\, h^2)^{3/2}\, e^{-\varepsilon_F/\, k_B T} \qquad (6.3)$$

where m_h is the hole mass. The product $n\,p$ is independent of the Fermi energy ε_F :

$$n\,p = 4\,(2\pi\ k_B\, T/\, h^2)^3\, (m_e\, m_h)^{3/2}\, e^{-\varepsilon_C/\, k_B T} \qquad (6.4)$$

So far, we only consider intrinsic semiconductors. Hence, we have

$$n = p = 2\,(2\pi\ k_B\, T/\, h^2)^{3/2}\, (m_e\, m_h)^{3/4}\ e^{-\varepsilon_C/\, 2\, k_B T} \qquad (6.5)$$

From (6.2) and (6.3) one obtains

$$m_e^{3/2}\ e^{-(\varepsilon_C\, -\, \varepsilon_F)/\, k_B T} \quad = m_h^{3/2}\, e^{-\varepsilon_F/\, k_B T} \qquad (6.6)$$

leading to

$$\varepsilon_F = \frac{\varepsilon_C}{2} + \frac{3}{4}\, k_B T \log(m_h/m_e) \qquad (6.7)$$

In the case $m_h = m_e$ we find $\varepsilon_F = \varepsilon_C/\, 2$, i. e., the Fermi energy is located in the middle of the energy gap.

Leaving the subject of the intrinsic semiconductors, we turn to the important case of the doped semiconductors, i. e., to the presence of donors (n-doping) or acceptors (p-doping). The energetic schematics is indicated in Fig. 6.2. It was the doping of semiconductors, which had opened the door to the many technical applications characterizing modern electronics.

The much smaller concentration of charge carriers in semiconductors compared to metals leads to important phenomena which are absent in metals. One of the first objects systematically studied (mainly by W. Schottky) was the metal-semiconductor contact (see Fig. 6.4). In order to establish equilibrium between both sides, electrons flow from the semiconductor into the metal (we assume an n-type semiconductor), and a positive space charge extending over a finite distance develops in the semiconductor. As a result a potential rise appears at the contact, which must be overcome by the electrons during current flow and which depends on the voltage V applied to the contact. The contact represents a rectifier, and the current I is given by

$$I = I_S\, (\, e^{eV/k_B T}\ -\ 1\,) \qquad (6.8)$$

I_S is the saturation current.

The p-n junction shown schematically in Fig. 6.5 is another important semiconductor device. It also shows rectifying behavior described again by Eq. (6.8). The p-n junction has found important applications in the junction transistor (see Fig. 6.6 b).

Finally, we mention that in semiconductors the thermoelectric effects are much larger than in metals, essentially since the Boltzmann distribution (6.1) is valid and the reduction factor $k_B T/\varepsilon_F$ of the Fermi-Dirac distribution is absent. The principle of Peltier cooling and a four-stage Peltier cascade is shown in Fig. 6.10.

7 Circling Electrons in High Magnetic Fields

Supplement

The behavior of an electric charge q moving in a magnetic field is dominated by the Lorentz force

$$\mathbf{f}_L = q\,\mathbf{v} \times \mathbf{B} \tag{7.1}$$

acting on the charge q moving with velocity **v** in the magnetic flux density **B** . From (7.1) we see that $\mathbf{f}_L$ is oriented perpendicular to both **v** and **B** , and that it results in a circular orbit of the charge (see Fig. 7.2). In the case of the electric current density (5.3) $\mathbf{j} = n\,(-e)\,\Delta\mathbf{v}_x$ flowing in x-direction through a conductor in the presence of a magnetic field oriented in z-direction, the Lorentz force points in y-direction $\mathbf{f}_{Ly} = q\ \Delta\mathbf{v}_x \times \mathbf{B}$. Here we have inserted the drift velocity $\Delta\mathbf{v}_x$ into (7.1). Due to $\mathbf{f}_{Ly}$ positive and negative electric charges accumulate at the two opposite edges of the conductor, respectively, (see Fig. 7.2 b) generating an electric field $\mathbf{E}_y$ in y-direction. Under stationary conditions the Lorentz force $\mathbf{f}_{Ly}$ is balanced by the electrostatic force $q\,\mathbf{E}_y$, and we have

$$q\ \Delta\mathbf{v}_x \times \mathbf{B} = q\,\mathbf{E}_y \tag{7.2}$$

yielding

$$|\mathbf{E}_y| = |\Delta\mathbf{v}_x \times \mathbf{B}| = \frac{1}{(-e)n}\ j\,B \equiv R_H\ j\,B \tag{7.3}$$

$\mathbf{E}_y$ is referred to as the Hall electric field, and we deal with the Hall effect. In (7.3) we have taken $q = -e$. The coefficient $R_H = \frac{1}{(-e)n}$ is the Hall constant (expected to be negative in the case of $q = -e$). We see that the Hall constant provides information on the concentration of the moving charge carriers. We note that the sign of the Hall electric field indicates the sign of the moving electric charges. During the early days a positive sign of the Hall constant had been observed sometimes, which represented a mystery (“anomalous Hall effect”) until the concept of holes in the electronic band structure was established.

As indicated schematically in Fig. 7.2 c , the Lorentz force also results in an increase of the electric resistivity in the presence of a magnetic field. At not too high magnetic fields this resistivity increment varies proportional to B^2 .

The quantum mechanical treatment of the electrons in the conduction band of a metal in the presence of a strong magnetic field, first given by L. D. Landau, takes into account that the Lorentz force (7.1) affects the energy spectrum of the electrons in an important way. Whereas in the absence of a magnetic field (B = 0) the energy spectrum is

$$\varepsilon = \frac{\hbar^2}{2m_e}\left(k_x^2 + k_y^2 + k_z^2\right) ; \quad B = 0 \tag{7.4}$$

in a magnetic field $B = B_z \neq 0$ assumed in z-direction the energy spectrum is changed to

$$\varepsilon = \hbar\omega_c\left(\ell + \frac{1}{2}\right) + \frac{\hbar^2}{2m_c}k_z^2 ; \quad B = B_z \neq 0 \tag{7.5}$$

Here, ℓ is an integer, m_c is the cyclotron mass of the electrons, and

$$\omega_c = \frac{e\,B}{m_c} \tag{7.6}$$

is the angular cyclotron frequency. In the presence of the magnetic field B_z the wave vectors k_x and k_y become irrelevant, and the corresponding states combine to a new state showing orbital motion. The states evenly filled in **k**-space in the absence of a magnetic field are now redistributed filling what are called Landau cylinders. An example is shown in Fig. 7.3. As we see from (7.5), the Landau cylinders are separated energetically from each other by the energy $\hbar\omega_c$, which increases proportional to B. At the magnetic field B = 1 T a typical value is $\hbar\omega_c \approx 10^{-4}$ eV.

The energy spectrum of the Landau cylinders is clearly displayed only if the orbital motion of the electrons remains unperturbed by collisions with phonons or impurities. So low temperatures and highly pure crystals are required for its experimental observation, and the condition

$$\omega_c\,\tau > 1 \tag{7.7}$$

must be satisfied, where τ is the scattering time. Furthermore, the thermal energy k_BT must be sufficiently small:

$$k_BT < \hbar\,\omega_c \tag{7.8}$$

Noting that the energy $\hbar\,\omega_c$ separating two neighboring Landau cylinders increases proportional to B, we see that with increasing magnetic field the number of Landau cylinders available for occupation up to the Fermi energy becomes smaller and smaller. As the

magnetic field is increased monotonically the redistribution of the electrons onto the Landau cylinders leads to a periodic oscillation of the total energy of the electrons, their energy passing through a minimum when $\varepsilon_F = \hbar\omega_c\, \ell$ and through a maximum when $\varepsilon_F = \hbar\omega_c\,(\ell + \frac{1}{2})$. As a result, other electronic properties such as, for example, the diamagnetism also oscillate as a function of the magnetic field.

The oscillation of the diamagnetism is referred to as the de Haas - van Alphen effect. It turns out that only the extremal cross sections of the Fermi surface taken perpedicular to the direction of **B** contribute to this effect. The contributions of all other parts of the Fermi surface drop out by cancelling each other.

The circular motion of the electrons in a magnetic field leads to another type of quantum effect in two-dimensional systems. In this case the Landau cylinders are reduced to Landau circles. Now we must look in more detail at the density of states w(**k**) in **k**-space. It is obtained by using periodic boundary conditions. Taking a crystal with the extension L along, say, the x-axis, the boundary condition requires that the wave e^{ikx} has the same values at x = 0 and x = L . Hence, we must have $e^{ikL} = 1$ or $kL = n\,2\pi$, wher n is an integer. The distance Δk between two consecutive k-values is $\Delta k = 2\pi/L$, and we find

$$w_1(k) = \frac{1}{\Delta k} = \frac{L}{2\pi} \tag{7.9}$$

Extending this to two dimensions, we obtain the density of states per unit area in **k**-space (excluding the electron spin)

$$w_2(k) = \left(\frac{L}{2\pi}\right)^2 \tag{7.10}$$

In the two-dimensional case the density of states per energy interval, $D_2(\varepsilon)$, is

$$D_2(\varepsilon) = w_2(k)\; 2\pi k \frac{dk}{d\varepsilon} = \left(\frac{L}{2\pi}\right)^2 2\pi k \frac{m}{\hbar^2 k} \tag{7.11}$$

and $D_2(\varepsilon)$ per unit area

$$D_2(\varepsilon) / L^2 = m / 2\pi\hbar^2 \tag{7.12}$$

The latter quantity is independent of the energy. Taking the energy interval $\hbar\,\omega_c$ between two Landau levels (from (7.5) with $k_z = 0$), the number of states per unit area and per Landau level is

$$N = [\, D_2(\varepsilon) / L^2 \,]\, \hbar\, \omega_c = \frac{e\,B}{h} \tag{7.13}$$

For the Landau quantum structure to be clearly observed, the conditions (7.7) and (7.8) must be satisfied. This case is shown schematically in Fig. 7.6.

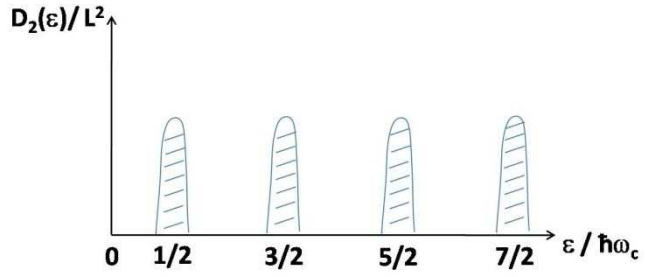

Figure 7.6: Density of states per unit area, $D_2(\varepsilon) / L^2$, plotted versus the normalized energy $\varepsilon / \hbar\,\omega_c$.

Turning now to the Hall effect (7.3), we find

$$E_y = \frac{1}{(-e)\,n_2}\, j_2\, B \tag{7.14}$$

where $j_2 = I/w$, with w being the width of the two-dimensional conductor. n_2 is the number of electrons per unit area. If the Fermi energy is located between two Landau levels, all Landau levels below (above) ε_F are occupied (unoccupied). In this case n_2 in (7.14) is given exactly by

$$n_2 = z\,N = z\,\frac{e\,B}{h} \tag{7.15}$$

where z is an integer. The Hall resistance R_{xy} is

$$R_{xy} = \frac{E_y}{j_2} = \frac{1}{z}\,\frac{h}{e^2} \tag{7.16}$$

R_{xy} depends only on the fundamental constants h and e , and we deal with the quantum Hall effect discovered by K. von Klitzing (see Figs. 7.1 and 7.4). For his experiment von Klitzing used the two-dimensional electron gas prepared at the surface of a metal-oxide-semiconductor field-effect transistor made from silicon.

The preparation of a two-dimensional electron gas for experiments in high magnetic fields continued to experience strong advances. Samples prepared at the interface between GaAs and $Al_xGa_{1-x}As$ became prominent, because in this material the fractional quantum Hall effect was discovered (see Fig. 7.5). A detailed theoretical discussion of this development is beyond the scope of our supplementary treatment.

8 The Winner: Superconductors

Supplement

The discovery of the Meissner effect in 1933 represented a turning point in the field of superconductivity, since it identified superconductivity as the result of a phase transition and it allowed to calculate the energy difference between the normal and the superconducting state. By carefully measuring the magnetic field near the exterior of a superconductor, Meissner had found that in the superconducting state an external magnetic field is expelled from a superconductor and that in its interior the magnetic field is zero (see Fig. 8.5).

Because of the Meissner effect, the superconducting state is established independent of the path along which this state is reached. In Fig. 8.13 we have marked with point c the superconducting state (below the critical temperature T_C and the critical magnetic field H_C). If we assume only infinite electric conductivity without the Meissner effect, along the path a→b→c the state with B = 0 will be established. On the other hand, along the path a→d→c the state with B ≠ 0 of point d will be reached. It is only because of the Meissner effect, that the state with B = 0 is always established independent of the previous path. (Here we have assumed perfect reversibility of the superconductor and have neglected flux trapping due to pinning). This demonstrates that superconductors are more than just mere perfect conductors (infinite conductivity); the Meissner effect defines in a unique way the property of the superconducting state.

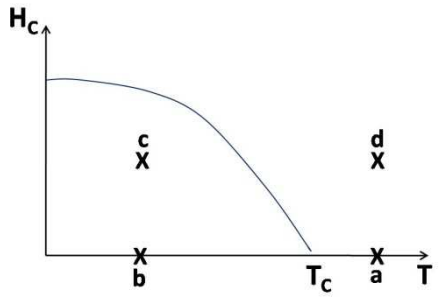

Figure 8.13: Path-independence of the superconducting state. Due to the Meissner effect, along the path a→d→c as well as along a→b→c the final state at point c with B = 0 is established.

The thermodynamic treatment of the superconducting phase transition, following the discovery of the Meissner effect and first carried out by Gorter and Casimir in 1934, deals with the Gibbs free energy density in the normal (G_n) and in the superconducting (G_s) state. At the magnetic field H we have

$$G_s(T,H) = G_s(T,0) - \int_0^H M(H)\, dH \qquad (8.1)$$

M(H) is the magnetization. In the case of the Meissner effect (perfect diamagnetism) it is

$$M(H) = -\frac{1}{4\pi} H \qquad (8.2)$$

The last term in (8.1) represents the work associated with the magnetic field expulsion. We obtain

$$G_s(T,H) = G_s(T,0) + \frac{1}{8\pi} H^2 \qquad (8.3)$$

Under equilibrium at $H = H_C(T)$ we have $G_n(T,H_C) = G_s(T,H_C)$ and on the other hand $G_n(T,H_C) = G_n(T,0)$. So in the case of $H = H_C$ we find

$$G_n(T,0) - G_s(T,0) = \frac{1}{8\pi} H_C^2(T) \qquad (8.4)$$

for the difference in energy density between the normal and the superconducting state.

The magnetic flux expulsion due to the Meissner effect is caused by a superconducting shielding current flowing at the surface of the superconductor. The magnetic field generated by this current exactly compensates the external magnetic field. This shielding surface current extends over a certain layer thickness at the surface, since its density must remain finite. Hence, the magnetic field reaches zero in the superconductor only at a certain depth λ_m referred to as the magnetic penetration depth. The density of the shielding current, j_s , is approximately given by

$$j_s = H_C / \lambda_m \qquad (8.5)$$

A phenomenological theory of the finite magnetic penetration depth λ_m was presented in 1935 by the brothers F. and H. London. For an outline of their theory we start with the force equation for an electron

$$m \frac{\partial \mathbf{v_s}}{\partial t} = (-e)\, \mathbf{E} \qquad (8.6)$$

without including a dissipative term. With the density of the superconducting current

$$\mathbf{j}_s = (-e)\, n_s\, \mathbf{v}_s \qquad (8.7)$$

we obtain

$$\mathbf{E} = [m / (e^2 n_s)] \frac{\partial \mathbf{j_s}}{\partial t} = \mu_o \lambda_m^2 \frac{\partial \mathbf{j_s}}{\partial t} \tag{8.8}$$

where λ_m (called also London penetration depth, and often denoted by λ_L) has been introduced in Eq. (8.5). λ_m can be expressed as

$$\lambda_m^2 = m / (\mu_o n_s e^2) \tag{8.9}$$

The quantities n_s and $\mathbf{v}_s$ are the density and the velocity of the superconducting electrons, respectively. μ_o is the magnetic permeability of free space. With the Maxwell equation

$$\text{curl } \mathbf{E} = - \frac{\partial \mathbf{B}}{\partial t} \tag{8.10}$$

we find from (8.8)

$$\mu_o \lambda_m^2 \text{ curl } (\frac{\partial \mathbf{j_s}}{\partial t}) + \frac{\partial \mathbf{B}}{\partial t} = 0 \tag{8.11}$$

It was the central idea of F. and H. London to extend (8.11) by removing the time derivative and thereby postulating the new equation

$$\mu_o \lambda_m^2 \text{ curl } \mathbf{j}_s + \mathbf{B} = 0 \tag{8.12}$$

With the Maxwell equation

$$\text{curl } \mathbf{H} = \mathbf{j} \tag{8.13}$$

we then obtain

$$\Delta \mathbf{H} = \frac{1}{\lambda_m^2} \mathbf{H} \tag{8.14}$$

yielding the solution

$$\mathbf{H}(x) = \mathbf{H}(0) \exp (-x / \lambda_m) \tag{8.15}$$

Here we consider the geometry of a superconductor filling the half-space with $x > 0$ and letting the coordinate x run (to the left) from the surface (at $x = 0$) into the interior of the superconductor. (**H** is assumed perpendicular to the x-direction).

Equations (8.8) and (8.12) are referred to as the first and the second London equation, respectively. In addition to the Maxwell equations they apply to superconductors and distinguish these substances from other materials. Equation (8.15) indicates that the magnetic field is exponentially screened from the interior of a superconductor, the screening taking place within a surface layer of thickness λ_m . As $T \rightarrow T_C$ we have $n_s \rightarrow 0$ and, hence, $\lambda_m \rightarrow \infty$.

In addition to the magnetic penetration depth, there exists a second important length in a superconductor, the coherence length ξ . This length represents the minimal spatial distance over which the superconducting property can change (spatial rigidity). The two lengths λ_m and ξ play an important role at the interface between a normal and a superconducting region (see Fig. 8.14).

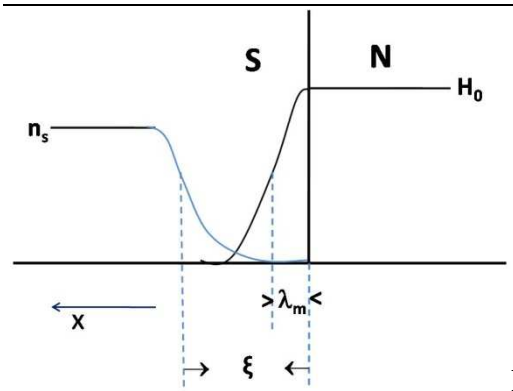

Figure 8.14: Variation of the density of the superconducting electrons, n_s , and of the magnetic field H with the distance from the interface between a normal (N) and a superconducting (S) region.

Because of the finite extension of the coherence length ξ , a superconducting region cannot exist right up to the border separating it from a normal region. Instead, it loses its superconducting property and, hence, the superconducting condensation energy, already at the distance ξ from the border. This results in the positive interface energy $\alpha' = (H_C^2 / 8\pi)\, \xi$. However, the amount $(H_C^2 / 8\pi)\, \lambda_m$ must be subtracted from this value, since within the magnetic penetration depth λ_m no gain and, hence, no loss in condensation energy appears. So for the wall energy α associated with an interface between a normal and a superconducting region one obtains

$$\alpha = (H_C^2 / 8\pi)\, (\xi - \lambda_m) \qquad (8.16)$$

Initially, one had thought that ξ would always be larger than λ_m , and that α would always be positive. However, around 1953 Abrikosov and Zavaritzkii for the first time discussed the

possibility that $\xi < \lambda_m$ and that α can become negative. They reasoned that if ξ and λ_m are material properties, the case of ξ being smaller than λ_m is a distinct possibility. Such considerations then lead to the important distinction between type-I (with $\xi > \lambda_m$) and type-II (with $\xi < \lambda_m$) superconductors.

In his subsequent theoretical analysis of type-II superconductivity Abrikosov made the important discovery of the Abrikosov flux-line lattice and of the superconducting mixed state (see Fig. 8.7). In the mixed state magnetic flux lines each carrying a single magnetic flux quantum penetrate into the superconductor, and the Meissner effect no longer exists. The mixed state appears above the lower critical magnetic field H_{C1} , and it exists up to the upper critical magnetic field H_{C2} .

Abrikosov had found the flux-line lattice as a solution of the equations of the Ginzburg-Landau theory of superconductivity. This theory describes the superconducting state in terms of a macroscopic quantum mechanical wave function. Quantization of the magnetic flux contained in the flux lines in units $h/2e = 2.068 \cdot 10^{-15}$ V s then results from the quantum condition that the wave function must reproduce itself exactly after one turn around the flux line. The magnetic flux lines are generated by superconducting currents circulating around their center. The radial dependence of the local magnetic field h, the density n_s of the superconducting electrons, and the superconducting current density j_s for an isolated flux line is shown schematically in Fig. 8.15.

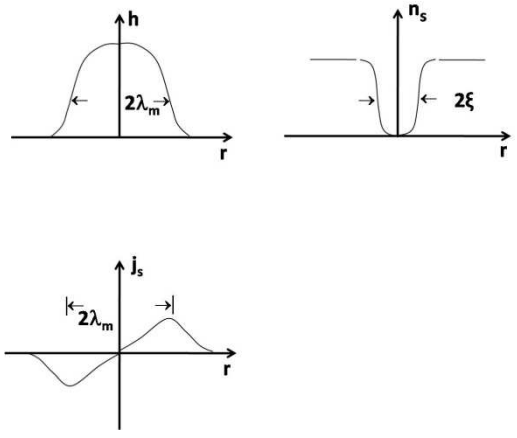

Figure 8.15: Structure of an isolated flux line. Local magnetic field h, density of the superconducting electrons n_s , and the circulating superconducting current density j_s versus the distance r from the axis of the flux line.

A direct experimental demonstration of the quantization of magnetic flux and of the magnetic flux quantum $h/2e$ as the smallest unit of magnetic flux in a superconductor has been given in 1961 and is indicated in Fig. 8.8. A detailed explanation of the step structure shown in Fig. 8.8b is illustrated in Fig. 8.16. Here, in part (a) the superconducting shielding current I_s is plotted versus the magnetic flux density B_e applied parallel to the axis of the small superconducting cylinder. The magnetic flux passing through the cross section of the cylinder $\pi R^2 B_e$ (R = cylinder radius) is given in units of the magnetic flux quantum $\varphi_o = h/2e$. (The vector $\boldsymbol{\varphi}_o$ is oriented along the direction of the flux density **B**). Initially, the shielding current I_s prevents the entry of magnetic flux into the cylinder bore (Meissner effect). When the magnetic field has reached the value $B_e = \varphi_o/(2\pi R^2)$, the shielding current I_s compensates exactly half a flux quantum $\varphi_o/2$ within the cylinder (point (1)). When B_e is increased further, the shielding current I_s reverses its sign (instead of continueing to grow), such that exactly one flux quantum φ_o exists in the cylinder (half of which is generated by I_s ; point (2)). During the further increase of B_e , $|I_s|$ decreases again until at $B_e = \varphi_o/(\pi R^2)$ the state with $I_s = 0$ is reached (point (3)). Upon the further increase of B_e this process repeats itself. In this way the steps in the number n of the magnetic flux quanta within the cylinder are generated (see Fig. 8.8b and Fig. 8.16b). The superposition of the applied magnetic field (solid arrows) and the magnetic field generated by I_s (dashed arrows) is shown schematically in Fig. 8.16c at the three points (1) – (3) indicated in Fig. 8.16a. Due to the entry of magnetic flux quanta φ_o into the cylinder the shielding current I_s and the kinetic energy associated with it remains limited.

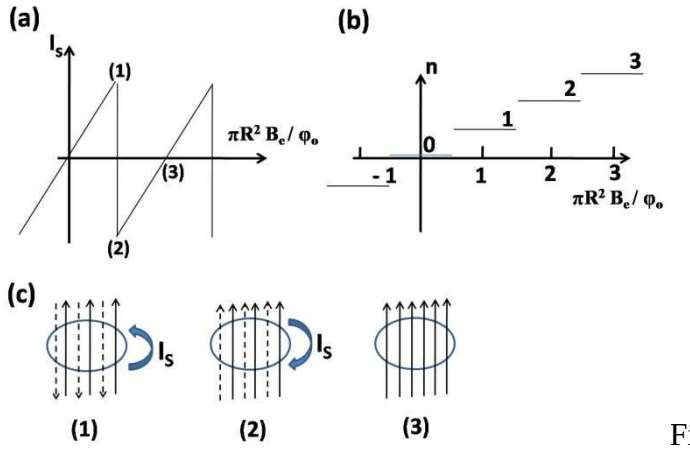

Figure 8.16: Experimental demonstration of the magnetic flux quantization based on the flux penetration into a small superconducting cylinder. Part (a) shows the superconducting shielding current I_s versus the magnetic flux density B_e applied parallel to the cylinder axis. Part (b) indicates the number n of the magnetic flux quanta within the cylinder versus B_e . Part (c) illustrates the superposition

of the applied magnetic field (solid arrows) and the magnetic field generated by I_s (dashed arrows) at the three points (1) – (3). Further details are given in the text.

In 1962 Josephson made his famous prediction that two weakly coupled superconductors (a "weak link" constituting what is now called a "Josephson junction") shows important effects described by the two Josephson equations

$$I_s = I_C \sin \chi \tag{8.17}$$

$$\frac{\partial \chi}{\partial t} = \frac{2e}{\hbar} V \tag{8.18}$$

Equations (8.17) and (8.18) are based on the concept, that superconductivity is a manifestation of a macroscopic quantum phenomenon that can be described in terms of an order parameter or a wave function

$$\psi = |\psi| e^{i\varphi} \tag{8.19}$$

characterized by an amplitude $|\psi(\mathbf{r}, t)|$ and a phase $\varphi(\mathbf{r}, t)$. The current-phase relation (8.17) indicates that the superconducting current I_s flowing across a weak link is related to the phase difference $\chi = \varphi_2 - \varphi_1$ between the two sides of the junction. I_C is the critical current of the particular junction geometry. The voltage-frequency relation (8.18) contains the important fact that a nonzero voltage V across the junction is always accompanied by a high-frequency oscillatory superconducting current flow across the junction. The Josephson equations (8.17) and (8.18) can be derived in different ways. One derivation due to Feynman starts from the time-dependent Schrödinger equation for the two wave functions ψ_1 and ψ_2 for the two separated superconductors, respectively, and introducing an additional coupling between both superconductors.

At the time the predictions by Josephson were highly surprising and met with severe criticism. In the meantime the "Josephson electronics" has developed into an important subject in physics and electrical engineering. The first experimental demonstration of the superconducting property of a weak contact between two superconductors was reported by Meissner and Holm in 1932. However, at the time it gained only little attention (except perhaps as an argument against Einstein's model of superconductivity based erroneously on "closed molecular chains" of the electrons).

In 1958 the BCS theory (named after Bardeen, Cooper, and Schrieffer) presented the first microscopic theory of superconductivity. Its main feature is the postulate of an attractive interaction between two conduction electrons of opposite momentum and spin resulting in the formation of electron pairs, so called Cooper pairs. The attraction between the two electrons is mediated by the vibrations of the atoms of the crystal lattice. An early clue that phonons would play an important role in superconductivity had been provided in 1950 by the discovery of the isotope effect in many superconducting elements. This effect says that the critical temperature T_C depends on the isotopic mass M of the lattice atoms following the relation

$$T_C \sim 1 / M^{\alpha} \qquad (8.20)$$

with the exponent $\alpha \approx 0.5$. Because of the total spin of an individual Cooper pair being zero, the Pauli principle does not apply, and all the Cooper pairs can occopy the same quantum state.

Another important prediction of the BCS theory is the existence of a gap in the energy spectrum of the electrons at the Fermi energy. An impressive demonstration of this energy gap has been given by Giaever in 1960 in his famous tunneling experiment (see Fig. 8.9).

The existence of magnetic flux lines each carrying a flux quantum $\varphi_o = h/2e$ in a type-II superconductor has important consequences for the resistive losses in these materials. In the presence of an applied electric current of density **j** each flux quantum experiences the Lorentz force $\mathbf{f}_L = \mathbf{j} \times \boldsymbol{\varphi}_o$. The resulting flux motion leads to dissipative losses and the generation of the flux-flow induced electric field

$$\mathbf{E} = - \mathbf{v}_{\varphi} \times \mathbf{B} \qquad (8.21)$$

Here, $\mathbf{v}_{\varphi}$ is the velocity of the flux-line motion. This flux-flow process obeys the force equation

$$\mathbf{j} \times \boldsymbol{\varphi}_o - \eta \mathbf{v}_{\varphi} = 0 \qquad (8.22)$$

where $\eta \mathbf{v}_{\varphi}$ is the dissipative term and η is a damping coefficient. In (8.22) the forces are given per unit length of flux line. From (8.21) and (8.22) one obtains the flux-flow resistivity as

$$\rho_f = \varphi_o B / \eta \qquad (8.23)$$

In the preceding discussion we have simplified the situation by ignoring the effects caused by flux pinning and by neglecting a force component leading to the flux-flow Hall effect.

9 The Big Surprise: High-temperature Superconductivity

Supplement

In the case of the cuprate (i.e. containing copper oxide) superconductors the formation of Cooper pairs has clearly been established again as the fundamental principle of the superconducting state. However, the microscopic pairing mechanism remains still undecided to date. In these materials the coherence length ξ is much shorter than in the classical superconductors. This small value of ξ , of the order of the dimension of the crystallographic unit cell, results in a high sensitivity of these materials to atomic defects and grain boundaries acting as effective centers of flux pinning (see Figs. 9.4 and 9.5).

The spatial symmetry of the wave function of the high-temperature superconductors describing the superconducting ground state of the Cooper pairs represents an important issue. It is well established that in the cuprates the wave function strongly varies with the spatial direction, and that it is dominated by the atomic d-orbital. This is generally expressed by plotting the wave function in the two-dimensional **k**-space associated with the CuO_2 planes. Such a polar plot is shown in Fig. 9.7 indicating the four leaves of the d-orbital alternately having positive and negative sign and displaying the nodes and antinodes as a function of the polar angle. The nodes and antinodes are fixed along the crystallographic directions as shown in Fig. 9.7 in the case of $d_{x^2-y^2}$ symmetry. For comparison, we also show the (isotropic) wave function with s-wave symmetry, encountered usually in the classical superconductors. A schematic of the CuO_2 planes for identifying the directions of the nodes and antinodes, respectively, is presented in Fig. 9.8 for the case of a square CuO_2 lattice.

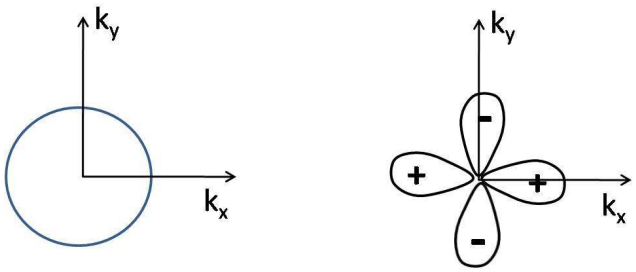

Fig. 9.7: **k**-space representation (k_x-k_y cross-section) of the superconducting wave function with s-wave symmetry (left) and $d_{x^2-y^2}$ symmetry (right). The latter symmetry dominates in the CuO_2 planes of the high-temperature superconductors.

The positive and negative sign of the $d_{x^2-y^2}$ wave function appearing at different polar angles, respectively, can have important consequences, if two crystals with different orientation are joined together with a well-defined grain boundary (bicrystal technique, see Fig. 9.5). The case where a positive lobe of the wave function encounters a negative lobe on the other side of the junction is referred to as a π-junction. A closed loop containing such a π-junction presents a challenge to the uniqueness of the wave function (frustration), since a sign change of the wave function remains after a complete rotation. In this case a half-integer magnetic flux quantum is spontaneously generated in this loop by a circular superconducting current (tricrystal experiment, see Fig. 9.6).

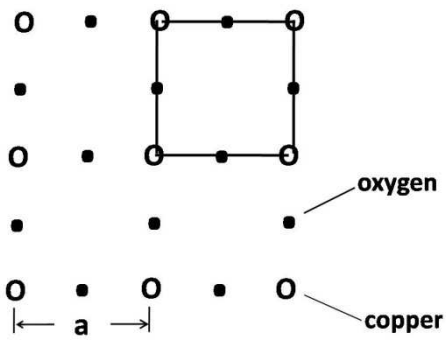

Fig. 9.8: A schematic of a square CuO_2 lattice. The unit cell is emphasized by heavy lines. The lattice constant a is indicated.

After MgB_2 superconducting material had been found in 2001, it became clear that the discovery of unexpected new superconducting materials is far from over. The most recent event was the report in January of 2008 from the group of Hideo Hosono in Japan, showing

the existence of superconductivity in a layered iron arsenide material with a transition temperature of 26 K. Subsequently, the study of this new class of high-temperature superconductors, referred to as iron pnictides, has been taken up worldwide with great intensity. In the meantime a transition temperature above 50 K has been observed. The information about this family of materials is accrueing fast and, to quote a recent report, “the situation changes daily”.

10 Magnetism: OrderAmong the Elementary Magnets

Supplement

In Chapter 7 we have discussed the oscillations of the diamagnetism due to the de Haas - van Alphen effect and the existence of the Landau cylinders in the energy spectrum of the electrons. Generally speaking, the diamagnetism results from the change of the orbital motion of the electrons in an external magnetic field. In this way it deals only with magnetic moments induced by the magnetic flux density **B**.

The magnetism of a material is quantified in terms of its magnetization **M**, defined as the magnetic moment per unit volume. **M** is given by the relation

$$\mathbf{M} = \chi \mathbf{B} \tag{10.1}$$

where χ is called the magnetic susceptibility. In the case of diamagnetism we have $\chi < 0$. In a magnetic field the electron orbits experience a precession motion at the Larmor frequency

$$\omega_L = e B / 2m \tag{10.2}$$

where m is the electron mass. As shown by Langevin, the Larmor precession motion of the electrons results in a negative magnetic susceptibility

$$-\chi \sim \langle r^2 \rangle \tag{10.3}$$

where $\langle r^2 \rangle$ is the average square of the radial extension of the electron distribution within the atom.

The magnetic moment of the electron spin results in paramagnetism. From the potential energy

$$U = -\boldsymbol{\mu} \cdot \mathbf{B} = -\mu B \cos\theta \tag{10.4}$$

of a magnetic moment $\boldsymbol{\mu}$ in the magnetic field **B** Langevin calculated the average $\langle \cos\theta \rangle$ from the classical Boltzmann distribution in the following way. (θ is the angle between the vectors $\boldsymbol{\mu}$ and **B**). According to Boltzmann, the statistical probability of the orientation of the magnetic moment $\boldsymbol{\mu}$ of the energy U is proportional to $\exp(-U/k_B T)$. Hence, one obtains (with the element $d\Omega$ of the solid angle)

$$\langle \cos\theta \rangle = \frac{\int \exp\left(-\frac{U}{k_B T}\right) \cos\theta \; d\Omega}{\int \exp\left(-\frac{U}{k_B T}\right) d\Omega} \tag{10.5}$$

$$= \frac{\int_0^\pi \exp(\mu B \cos\theta / k_B T)\, 2\pi \sin\theta \cos\theta \; d\theta}{\int_0^\pi \exp(\mu B \cos\theta / k_B T)\, 2\pi \sin\theta \, d\theta} \tag{10.6}$$

and after a few steps

$$\langle \cos\theta \rangle = \coth x - \frac{1}{x} \equiv L(x); \quad x = \mu B / k_B T \tag{10.7}$$

L(x) is referred to as the Langevin function. The average magnetization $\langle M \rangle$ is

$$\langle M \rangle = N \mu \langle \cos\theta \rangle = N \mu \, L(x) \tag{10.8}$$

where N is the number of elementary magnetic moments μ per unit volume. A plot of L(x) is shown in Fig. 10.6.

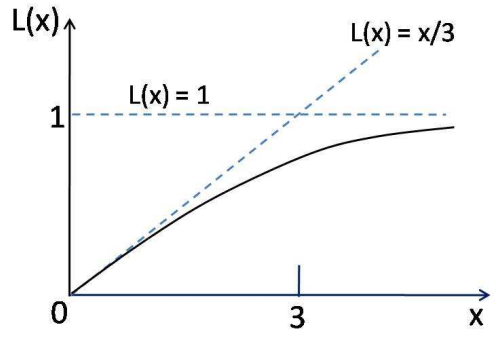

Fig. 10.6: Langevin function L(x) defined in (10.7).

In the case $x << 1$ (high temperatures) we have $L(x) \approx x / 3$, and we obtain

$$\langle M \rangle = N \mu^2 B / 3 k_B T = \frac{C}{T} B \qquad (10.9)$$

This is Curie's law, and $C = N \mu^2 / 3 k_B$ is referred to as Curie's constant. On the other hand, in the case $x >> 1$ (low temperatures) the magnetization saturates. We note that paramagnetism deals with the reorientation of existing magnetic moments in an external magnetic field.

Whereas the result of Eq. (10.8) was obtained based on the concepts of classical physics, within the framework of quantum theory the quantization of the direction of the elementary spin must be taken into account. According to quantum theory, the magnetic moment of an isolated atom is

$$\boldsymbol{\mu} = - g \mu_B \mathbf{J} / \hbar \qquad (10.10)$$

Here

$$\mu_B = e \hbar / 2 m \qquad (10.11)$$

is the Bohr magneton. **J** is the total angular momentum given by the vector sum of the orbital (**L**) and the spin (**S**) angular momentum:

$$\mathbf{J} = \mathbf{L} + \mathbf{S} \qquad (10.12)$$

The factor g is the Landé g-factor

$$g = 1 + \frac{J(J+1) + S(S+1) - L(L+1)}{2 J (J+1)} \qquad (10.13)$$

In a magnetic field the quantized energy levels of an elementary magnetic moment are

$$U = m_J g \mu_B B \; ; \quad m_J = J, J-1, J-2, \cdots, -J \tag{10.14}$$

For a single spin and $L = 0$ we have $m_J = \pm ½$ and $g = 2$:

$$U = \pm \mu_B B \tag{10.15}$$

In thermal equilibrium the magnetization of this two-level system is

$$\langle M \rangle = N \mu_B \tanh x \; ; \quad x = \mu_B B / k_B T \tag{10.16}$$

In the limit $x << 1$ (high temperatures) we obtain

$$\langle M \rangle = N \mu_B^2 B / k_B T \tag{10.17}$$

which is similar to Curie's law.

In the general case, with $2J + 1$ energy levels according to (10.14), in thermal equilibrium the magnetization is

$$\langle M \rangle = N \mu_B B_J(x) \; ; \qquad x = \mu_B B / k_B T \tag{10.18}$$

The function $B_J(x)$ is referred to as the Brillouin function (not shown here). In the limit $x << 1$ (high temperatures) the form of the Curie law $\langle M \rangle \sim B/T$ is obtained again.

The paramagnetism of the conduction electrons in metals represents a special case. Because of the validity of Fermi statistics only the fraction $k_B T/\varepsilon_F$ of the conduction electrons contribute to paramagnetism. Multiplying (10.17) with this factor, we obtain

$$\langle M \rangle = N \mu_B^2 B / \varepsilon_F \tag{10.19}$$

and the proportionality to T^{-1} has disappeared. This result is somewhat similar to the case of the specific heat of the conduction electrons we have discussed in Chapter 5 and its Supplement.

In the case of diamagnetism and paramagnetism we were dealing with the response of a system of magnetic moments to an external magnetic field. Next we turn to another magnetic phenomenon, namely the spontaneous order among magnetic moments in the absence of an external magnetic field: ferromagnetism.

The complete theory of ferromagnetism had to await the advent of quantum mechanics. However, a phenomenological theory was developed already in 1907 by Pierre Weiss. He postulated the existence of an effective magnetic field within the crystal ("Weiss field") reaching high values up to 10^3 Tesla. It is this effective magnetic field which then causes the spatial ordering of the individual atomic or molecular magnetic moments.

For the Weiss field B_W we assume $B_W = \lambda M$, where λ is a constant independent of the temperature. In a cooperative way each individual magnetic moment experiences the average magnetization of all the others ("mean-field approximation"). The ferromagnetic order persists up to the Curie temperature T_{CU}, above which the ferromagnetic order disappears and the crystal becomes paramagnetic. Looking at the paramagnetic state (above T_{CU}) in the presence of an external magnetic field B_a, we have

$$M = \chi_p (B_a + B_W) = \chi_p (B_a + \lambda M) \qquad (10.20)$$

with the paramagnetic susceptibility $\chi_p = C / T$. From (10.20) we obtain

$$M \left(1 - \frac{C}{T} \lambda\right) = \frac{C}{T} B_a \qquad (10.21)$$

and

$$\chi = M / B_a = C / (T - T_{CU}) \; ; \; T_{CU} \equiv C \lambda \; ; \; (T \rightarrow T_{CU} \text{ from above}) \qquad (10.22)$$

This is the Curie-Weiss law with χ^{-1} being linear in T. A more accurate treatment yields

$$\chi = C / (T - T_{CU})^{1.33} \; ; \; (T \rightarrow T_{CU} \text{ from above}) \qquad (10.23)$$

in agreement with experiment.

It was W. Heisenberg, who in 1928 presented the first quantum mechanical theory of ferromagnetism. He introduced the concept of the exchange interaction between two atoms 1, 2 having the spin $\mathbf{S}_1$, $\mathbf{S}_2$, resulting in the exchange energy (Heisenberg model)

$$U = - 2 J \mathbf{S}_1 \cdot \mathbf{S}_2 \qquad (10.24)$$

with the exchange integral

$$J = \iint d\,\mathbf{r}_1 \; d\,\mathbf{r}_2 \; \psi_a^*(\mathbf{r_1}) \, \psi_b^*(\mathbf{r_2}) \, V(\mathbf{r}_1 - \mathbf{r_2}) \, \psi_{\mathbf{a}}(\mathbf{r_2}) \, \psi_b(\mathbf{r}_1) \qquad (10.25)$$

In the case of ferromagnetism we have $J > 0$, and the parallel spin orientation is energetically favored. The exact theoretical calculation of the exchange integral J requires a detailed treatment.

For obtaining the temperature dependence of the magnetization M we use the "mean field approximation" $B_W = \lambda M$. For a two-level system ($S = ½$) we find from (10.16)

$$M = N \mu_B \tanh (\mu_B \lambda M / k_B T) \qquad (10.26)$$

Introducing the quantities $m \equiv M / (N \mu_B)$ and $t \equiv T / T_{CU} = k_B T / (N \mu_B^2 \lambda)$ we obtain

$$m = \tanh (m / t) \qquad (10.27)$$

(Here we have noted $T_{CU} = C \lambda$, with $C = N \mu_B^2 / k_B$ according to (10.17)). The transcendental equation (10.27) can be solved graphically as indicated schematically in Fig. 10.7 . In this way the temperature dependence of the magnetization shown in Fig. 10.8 is found. It corresponds to that of a second-order phase transition, where the magnetization plays the role of the order parameter.

Usually, the saturation value of the magnetization at $T \rightarrow 0$ is strongly reduced due to the appearance of individual ferromagnetic domains with different orientation, as shown schematically in Fig. 10.2.

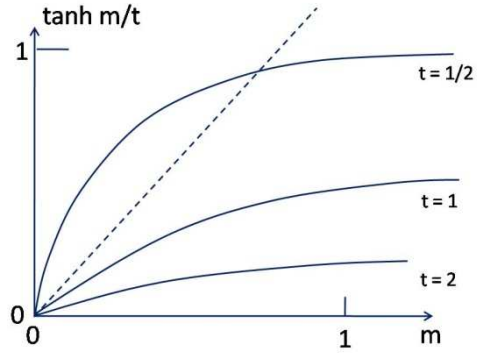

Fig. 10.7: Schematics of the graphical solution of the transcendental equation (10.27). At the critical point t = 1 the intersection is located at m = 0. In the case $t \rightarrow 0$ the intersection moves toward $m = 1$.

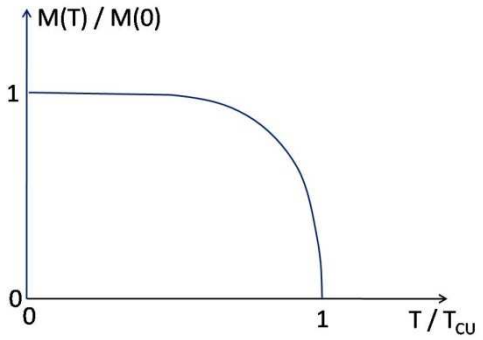

Fig. 10.8: Normalized magnetization (saturation value) plotted versus T / T_{CU} .

Deviations from the ferromagnetic ground state in the limit of zero temperature, where all spins are oriented exactly parallel to each other, are due to the thermal excitation of spin waves (see Fig. 10.1). Looking at a linear chain of N spins, all oriented parallel to each other, according to (10.24) the total energy is

$$U = - 2 J \sum_{p=1}^{N} \mathbf{S}_p \ \mathbf{S}_{p+1} \qquad (10.28)$$

yielding the energy of the ground state

$$U_O = - 2 N J S^2 \qquad (10.29)$$

As a possible excitation we consider the case where a single spin becomes oriented antiparallel to its neighbors (Fig. 10. 1 b). The energy increase ΔU is

$$\Delta U = 2 J (2S^2 + 2S^2) = 8 J S^2 \qquad (10.30)$$

(where in the bracket we have indicated the interaction with the left and right neighbor seperately). Only a much smaller excitation energy is needed, if the change of the spin orientation occurs gradually, and this is realized in terms of the spin waves (Fig. 10.1 c). Spin waves represent oscillations of the spin orientation, the oscillations possessing the quantized energy $\hbar \omega$. These quantized energies are referred to as magnons. In the case of ferromagnetic magnons the dispersion relation is obtained from the equation for the temporal change of the angular momenta of the spins. In the limit of small excitation amplitudes one finds the dispersion relation

$$\hbar \omega = 4 J S (1 - \cos ka) \qquad (10.31)$$

where a is the lattice constant of the chain and k the wave number. In the limit of long wavelengths ($ka << 1$) Eq. (10.31) yields

$$\hbar\,\omega = 2\,J\,S\,a^2\,k^2 \qquad (10.32)$$

We note $\omega \sim k^2$, in contrast to the case of phonons, where $\omega \sim K$ (see (3.7) and (3.8)).

The extension of these results to a three-dimensional lattice is straightforward.

The thermal excitation of magnons follows the Bose-Einstein distribution law (3.2). The energy of the magnons is

$$U = \int d\omega\, D(\omega) < n_\omega > \hbar\,\omega \qquad (10.33)$$

(analogous to (3.3)), where the integral extends over the 1. Brilouin zone. In the limit of low temperatures (ka << 1) one finds $D(\omega) \sim \omega^{1/2}$ and $U \sim T^{5/2}$. For the magnon specific heat this yields

$$C_V = \left(\frac{\partial U}{\partial T}\right)_V \sim T^{3/2} \qquad (10.34)$$

The thermal excitation of magnons reduces the magnetization by the amount $\Delta M = M(0) - M(T)$. One finds (F. Bloch 1931)

$$\Delta M / M(0) \sim T^{3/2} \qquad (10.35)$$

In addition to the parallel spin orientation of the ferromagnetic order, there exists antiferromagnetism with antiparallel spin orientation between the neighbors. In this case the exchange integral (10.25) is negative. There exist also antiferromagnetic spin waves, having the dispersion relation

$$\hbar\,\omega = 4\,|\,J\,|\;S\;|\sin ka\,| \qquad (10.36)$$

similar to the case of phonons (see (3.7)). In the limit ka << 1 this yields

$$\hbar\,\omega = 4\,|\,J\,|\;S\;|\,ka\,| \qquad (10.37)$$

The contributions of the antiferromagnetic magnons to the specific heat and to the heat conductivity varies proportional to T^3 in the limit of low temperatures.

In the technical applications of ferromagnetic materials the magnetic “hardness” represents an important quality, and one distinguishes between magnetically soft and hard materials. The magnetic hardness is quantified in terms of the “coercive force”. The latter represents the magnitude H_C of the magnetic field, at which the unmagnetized state of the material is reestablished again, if this magnetic field is applied a second time in a direction opposite to that of the original magnetization. This situation is shown schematically in Fig. 10.9 , where

the magnetic flux density B is plotted versus the applied magnetic field H in the case of a magnetically soft and hard material. A soft material displays a small value of H_C and weak hysteresis, whereas a hard material shows a large value of H_C and strong hysteresis.

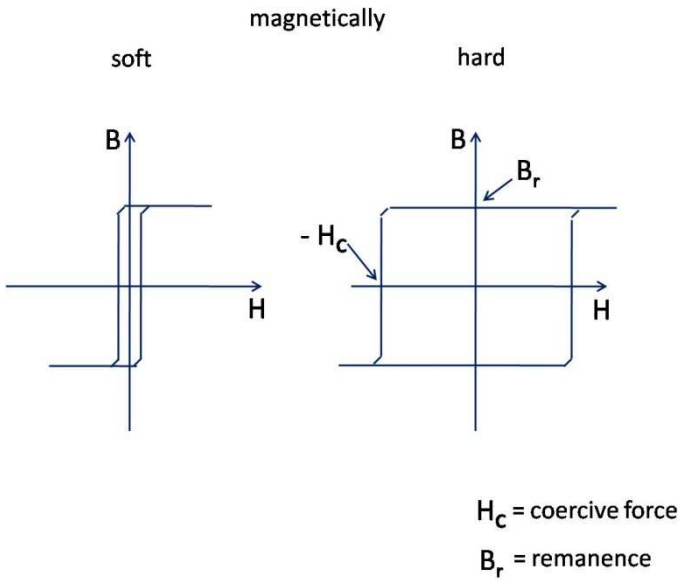

Fig. 10.9: Magnetic flux density B versus the applied magnetic field H in the case of a magnetically soft (left side) and magnetically hard (right side) material.

11 Nanostructures: Superlattices, Quantum Wires, and Quantum Dots

Supplement

As we have discussed in Chapter 2 and its Supplement, in a crystal lattice the elementary cell repeats itself in all three spatial directions, generating a three-dimensional periodic structure. This principle has been extended in the case of superlattices, where the composition of a material is periodically modulated along one spatial direction (see Fig. 11.2). Such multi-layered structures are fabricated using modern thin-film technology.

In the Supplement of Chapter 2 we have introduced the concept of the reciprocal lattice in wave-vector space (**k**-space) and its partition into Brillouin zones (Fig. 2.11). In Chapter 4 and its Supplement we have seen that Bragg reflection (Fig. 4.6) occurs, if the wave vector **k**

of the electrons reaches the boundary of a Brillouin zone, resulting in the forbidden gaps in the energy spectrum of the electrons (Fig. 4.2 and 4.3).

In the example shown in Fig. 2.11 Bragg reflection occurs at the values $k_x = \pi/a$ and $k_y = \pi/b$ of the wave vector **k** , where a and b are the lattice constants in x- and y-direction, respectively. In a superlattice, along the direction of its modulation, the (super)-lattice constant is much larger than the lattice constant of the underlying crystal lattice. Hence, Bragg reflection is expected at a correspondingly much smaller value of the electron wave vector than the electron wave vector in crystal lattices, leading to relatively narrow energy bands ("minibands"). It was the existence of these minibands and the new expected electrical properties of the superlattices, which had motivated the research in this field.

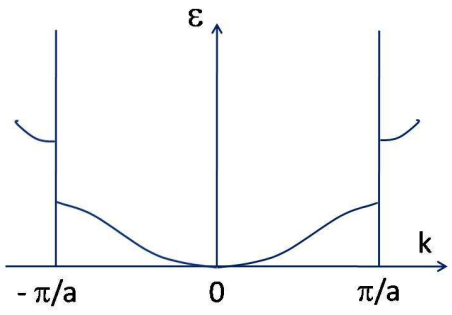

Fig. 11.9: Energy spectrum ε(k) in the 1. Brillouin zone extending between $k = \pi/a$ and $k = -\pi/a$.

We consider a one-dimensional periodic chain of atoms with the lattice constant a . The energy spectrum between the boundaries of the 1. Brillouin zone, π/a and $-\pi/a$, is shown in Fig. 11.9. Starting from the force equation (5.1), we write

$$\left|\frac{\Delta k}{\Delta t}\right| = e\,E / \hbar \qquad (11.1)$$

In the absence of any scattering process, the electron (or hole) gains momentum and energy in the electric field until the value $k = \pi/a$ is reached. Then the electron is transferred from $k = \pi/a$ to $k = -\pi/a$ by means of Bragg reflection. At this point the wave vector increases again due to the force equation (5.1), and this process repeats itself resulting in periodic oscillations of the electron (so called Bloch oscillations). Denoting the time $\Delta t \equiv \tau_B$ it takes to increase the wave vector by the amount $\Delta k = 2\pi/a$ corresponding to one cycle, we obtain from (11.1)

$$2\pi/a = e\,E\,\tau_B / \hbar \qquad (11.2)$$

and

$$\omega_B \equiv 2\pi/\tau_B = e\,E\,a/\hbar \qquad (11.3)$$

The angular frequency ω_B represents the Bloch frequency. For the occurrence of the Bloch oscillations the mean electron scattering time τ must be sufficiently long, satisfying the condition

$$\omega_B \tau >> 1 \qquad (11.4)$$

We see that for this phenomenon to appear we need highly pure materials and low temperatures. Another important prerequisite is the realization of a large lattice constant a , which leads to a small energy width of the miniband and a correspondingly large value of ω_B according to (11.3). In the energy bands of typical crystals the electrons always experience a scattering process before they reach energetically the upper band edge in an electric field, and Bloch oscillations are rendered impossible (see Fig. 11.3) by the intervening scattering mechanisms.

The possible generation of Bloch oscillations in superlattices results from the quantum mechanical wave properties of the conduction electrons (like many other effects). A different manifestation of these wave properties arises in the case of electrical conductors with smaller and smaller dimensions fabricated by means of modern nanotechnology. Eventually, mesoscopic length scales are obtained, within which no scattering processes occur any more (ballistic propagation, see Fig. 11.1 and 11.4).

The first treatment of ballistic electron transport in mesoscopic conductors (quantum wires) is due to Landauer. We briefly outline the central idea. The quantum wire is assumed to be placed along the x-direction. At both ends it is connected to electrodes with the energies $\varepsilon + ½\ eV$ and $\varepsilon - ½\ eV$, respectively. Here V is the electric potential difference between both electrodes. Treating both electron spins seperately, the current is

$$I = -2e \int \frac{dk_x}{2\pi}\, v_x \left[f\left(\varepsilon + \frac{1}{2}eV, \varepsilon_F\right) - f\left(\varepsilon - \frac{1}{2}eV, \varepsilon_F\right) \right] T_{trm} \qquad (11.5)$$

Here we have used the abbreviation for the Fermi distribution function (5.10)

$$f(\varepsilon, \varepsilon_F) \equiv \frac{1}{e^{(\varepsilon-\varepsilon_F)/k_B T} + 1} \qquad (11.6)$$

and considered the current flow in both directions (+ x and – x). The quantity T_{trm} is a transmission coefficient containing the electron scattering processes establishing the equilibrium with the local electrochemical potential of the electrodes. In the quantum wire itself scattering processes are assumed to be absent. If the voltage V and the temperature is small, we have

$$\left[f\left(\varepsilon + \frac{1}{2}eV, \varepsilon_F\right) - f(\varepsilon - \frac{1}{2}eV, \varepsilon_F) \right] = \left(\frac{\partial f}{\partial \varepsilon}\right)_{V=0} eV \qquad (11.7\ a)$$

$$= -\delta(\varepsilon - \varepsilon_F)\, eV \qquad (11.7.b)$$

where $\delta(x)$ is the Dirac delta function. Using $v_X\, dk_X = (1/\hbar)d\varepsilon$ we finally obtain for the conductance G

$$G = \frac{I}{V} = \frac{2e^2}{h} T_{trm} = 2\, G_O\, T_{trm} \qquad (11.8)$$

The quantity $G_O = e^2/h$ represents the quantum unit of conductance.

12 Defects in the Crystal Lattice: Useful or Harmful ?

Supplement

A certain degree of disorder must always exist in a crystal by virtue of fundamental considerations. In the following we present the thermodynamic arguments for the ineluctable presence of lattice defects, taking the example of lattice vacancies. A vacancy is a location in the crystal, where an atom of the lattice is mising.

We start with the free enthalpy of the crystal

$$G = U + p\,V - T\,S \qquad (12.1)$$

(U = internal energy; p = pressure; V = volume; T = temperature; S = entropy). From (12.1) we see that an increase of the entropy (caused by disorder) reduces the free enthalpy. Because of the TS term in equation (12.1), the reduction of the free enthalpy becomes more and more important at high temperatures. This is exactly the reason for the appearance of disorder at thermodynamic equilibrium in the crystal.

We consider a crystal with N identical atoms. Due to the presence of n lattice vacancies the free enthalpy G changes by the amount

$$\Delta G(n, p, T) = n\,U_A + n\,p\,V_A - n\,T\,S_A^{vibr} - T\,(N + n)\,S_m \qquad (12.2)$$

The proportionality to n of the terms in equation (12.2) is valid only for values of n that are small relative to N, i.e., $n << N$. Here U_A = activation energy of vacancy formation; V_A = activation volume of vacany formation; S_A^{vibr} = change of the entropy of the lattice vibrations per vacancy; S_m = mixing entropy of the particles. The mixing entropy per particle is defined as

$$S_m = - k_B \cdot \sum_j x_j \ln x_j \qquad (12.3)$$

where x_j is the atomic fraction of the component j . In the case of vacancies we have

$$S_m = - k_B \frac{n}{n+N} \ln \frac{n}{n+N} - k_B \frac{N}{n+N} \ln \frac{N}{n+N} \qquad (12.4\,a)$$

$$\approx - k_B \frac{n}{N} \ln \frac{n}{N} + k_B \ln\left(1 + \frac{n}{N}\right) \qquad (12.4\,b)$$

$$\approx - k_B \left(\frac{n}{N} \ln \frac{n}{N} - \frac{n}{N}\right) \qquad (12.4\,c)$$

(using again the approximation valid in the case $n << N$). In the case of equilibrium:

$$\left(\frac{\partial\,\Delta G}{\partial n}\right)_{p,T} = U_A + p\,V_A - T\,S_A^{vibr} + k_B T \ln \frac{n}{N} = 0 \qquad (12.5)$$

and

$$c(p, T) \equiv \frac{n(p,T)}{N} = \exp(S_A^{vibr}/k_B) \cdot \exp[-(U_A + pV_A) / k_B T] \qquad (12.6)$$

From (12.6) we see that plots of log c versus 1/T or versus p yield straight lines (see Fig. 12.6). From the slope of the plot versus 1/T one obtains $U_A + p\,V_A$ (where the second term generally can be neglected at p = 1 at). From the slope of the plot versus p one obtains V_A.

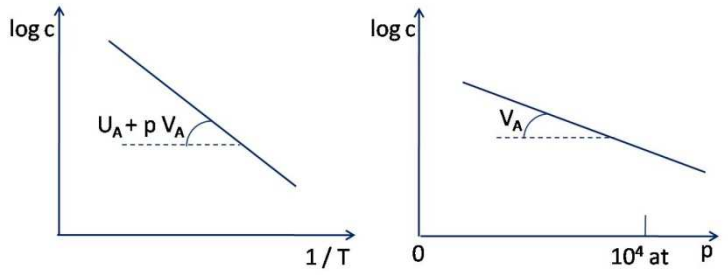

Fig. 12.6: Plots of log c versus 1/T (left) and versus p (right), schematically according to Eq. (12.6).

The strongly temperature dependent spontaneous generation of lattice vacancies under thermodynamic equilibrium contributes also to the volume expansion of a crystal, in addition to the standard phenomenon of thermal expansion. This effect has been demonstrated in famous experiments by Simmons and Baluffi, who compared the measured relative length change, $\Delta L/L$, of a crystal with the relative change of the lattice constant, $\Delta a/a$, obtained from X-ray diffraction. In Fig. 12.2 we show their measurements in the case of an aluminum sample.

Lattice vacancies are able to move within the crystal by means of diffusion. During an elementary diffusion jump from one lattice site to another vacancies pass through an activated state (located between two neighboring lattice sites). Denoting the number of vacancies in the activated state by n^*, one obtains for the ratio n^*/n an expression analogous to (12.6), where the activation energy of motion, U_B, the activation volume of motion, V_B, and the change of the vibrational entropy, S_B^{vibr}, appear:

$$n^*/n = \exp(S_B^{vibr}/k_B) \cdot \exp[-(U_B + pV_B) / k_BT] \qquad (12.7)$$

The temperature (and pressure) dependent concentration and mobility of lattice vacancies plays a crucial role in all diffusion processes in crystals and represents a key quantity of solid state chemistry.

In Chapter 12 other types of lattice defects such as interstitials, color centers, and dislocations are briefly discussed.

Glossary (Electrons in Action)

Abrikosov Flux-Line Lattice: regular geometric arrangement of quantized magnetic flux lines (vortices) in a superconductor oriented along the direction of the externally applied magnetic field. It exists in a → type-II superconductor in the mixed state at intermediate magnetic fields between the lower (at which magnetic flux lines start to appear in the superconductor) and the upper critical magnetic field (at which superconductivity vanishes).

Aharonov - Bohm Effect: effect in a small multiply connected object (ring or cylinder) due to the → interference between the quantum mechanical wave function of an electron in the different parts of the object.

Antiferromagnetism: caused by the spontaneous antiparallel orientation of the spin magnetic moments of the neighboring atoms or molecules in a crystal.

Ballistic Propagation: undisturbed propagation of a particle/wave without experiencing a scattering process between source and detector.

Barkhausen Jumps: discontinuous change of the magnetization of individual ferromagnetic domains during variation of an external magnetic field.

BCS Theory: microscopic theory of superconductivity developed by John Bardeen, Leon Cooper, and Robert Schrieffer. It assumes that two conduction electrons are bound together forming → Cooper pairs, which obey → Bose-Einstein statistics and occupy a common ground state. The energy of the ground state is separated by an energy gap from the normal-state energy of the electrons. In a Cooper pair the attraction between the two electrons is effected by the → phonons in the superconductor.

Bitter Decoration Technique: method for the experimental observation of magnetic domain structures. It was introduced by the American Francis Bitter and works by sprinkling, say, small ferromagnetic particles on the surface of the sample. The particles then accumulate at the locations at the surface, where the local magnetic field shows a strong spatial variation, for example, at the domain boundaries.

Bloch Ansatz: approximation of the quantum mechanical wave function of the electrons in a crystal in terms of the bound states of the atoms at the individual lattice sites of the crystal, in the case when a hopping process of the electrons between the sites occurs only rarely.

Bloch Oscillation: oscillatory motion of the conduction electrons within a narrow → energy band due to an electric field, caused by → Bragg reflection at the crystal lattice when the electrons reach the energy of the upper band edge.

Bloch Wall: region in a magnetic material between two magnetic domains, in which the spin magnetic moment rotates from the direction in a magnetic domain to the different direction in the neighboring domain.

Boltzmann Statistics: applies to (classical) particles or objects, which can be distinguished from each other. It leads to the Boltzmann distribution of the number $<N_j>$ of particles having the energy E_j :

$$<N_j> = N \frac{e^{-E_j/k_BT}}{\sum_j e^{-E_j/k_BT}}$$

N is the total number of particles. k_B is Boltzmann's constant. e^{-E_j/k_BT} is referred to as the Boltzmann factor.

Bose-Einstein Statistics: applies to elementary particles, which are identical and, hence, are indistinguishable from each other, and which have zero or integer intrinsic angular momentum or spin. These particles are referred to as "bosons". Examples are → photons, → phonons, α-particles (helium nuclei), and the → Cooper pairs. The statistical average <N(E)> of the occupation number N in the case of the Bose-Einstein statistics is

$$<N(E)> = \frac{1}{e^{(E-\mu)/k_BT} - 1}$$

(E = energy; μ = → chemical potential). In the limit $(E - \mu) >> k_BT$ the Bose-Einstein distribution approaches the → Boltzmann distribution.

Bragg Reflection: when in an electric field the conduction electrons reach the energy of the upper band edge, they decelerate and reverse their velocity. This process results from the interaction of the electrons with the periodic potential of the crystal lattice and is referred to as Bragg reflection. It is named after William Henry and William Lawrence Bragg (father and son), who had analyzed the → diffraction of X-rays by a crystal lattice.

Carbon Nano Tube: narrow cylinder formed by carbon atoms. There exist single-wall and multi-wall carbon cylinders.

Chemical Potential: it represents the energy per particle in a system of particles (electrons, atoms, molecules). At equilibrium it is the same for all particles in the system. In the case of electrons in a solid, in the limit of zero temperature the chemical potential μ is equal to the → Fermi energy ε_F ($\mu = \varepsilon_F$).

Coherence Length of a Superconductor: minimum distance over which a material can change its superconducting property.

Conduction Band: highest → energy band which is only partly filled with electrons.

Cooper Pair: pair of two conduction electrons bound together by an attractive interaction. Cooper pairs represent the key element of the → BCS theory of superconductivity.

Critical Magnetic Field and Critical Temperature of a Superconductor: value of the magnetic field and of the temperature, above which superconductivity vanishes.

Curie Law: it was discovered by Pierre Curie and states that in a → paramagnet the magnetic moment changes proportional to the inverse temperature.

Cyclotron Motion: circular motion of electric charge carriers at the cyclotron frequency ν_C in a magnetic field due to the action of the → Lorentz force.

Debye Model of the Specific Heat: it assumes the existence of a continuous frequency range of → phonons in a crystal from zero frequency up to a maximum frequency (phonon spectrum) and takes into account the variation of the number of phonons occupying the modes of the different phonon frequencies with the temperature.

de Haas – van Alphen effect: oscillatory dependence of the → diamagnetism upon the magnetic field due to the energy quantization of the conduction electrons in the form of the → Landau cylinders .

Diamagnetism: caused by the magnetic moment due to the orbital motion of the electrons in a magnetic field.

Diffraction: causes the change of the direction of a propagating wave due to the interaction of the wave with an object or a geometric arrangement of objects.

Dislocation: perturbation of the perfect order of a crystal lattice by an additional atomic plane ending within the crystal. Around a dislocation the crystal lattice is distorted. Dislocations strongly influence the mechanical strength of a material.

Einstein Model of the Specific Heat: it assumes a single vibrational frequency ν_E of the lattice atoms in a crystal and takes into account the variation of the number of → phonons occupying this mode with the temperature.

Electric Potential Gradient: spatial slope of the potential energy of an electric charge in an electric field. The electric potential difference between two points is referred to as the voltage between the points.

Energy Bands: they describe the dependence of the energy of the electrons in a crystal upon their mechanical momentum. The exactly periodic structure of the crystal lattice results in forbidden ranges of the energy. The allowed energy ranges separated in this way from each other are referred to as energy bands.

Exciton: pair of a (negative) electron and a (positive) hole in a semiconductor bound to each other.

Fermi-Dirac Statistics: applies to elementary particles, which are indistinguishable from each other, and which have half-integer intrinsic angular momentum or spin. These particles are referred to as "fermions". An important example are electrons (with spin ½). Fermions must satisfy the Pauli exclusion principle, which states that each quantum mechanical state of a system can be occupied at most only by a single particle. The statistical average <N(E)> of the occupation number N in the case of the Fermi-Dirac distribution is

$$<N(E)> = \frac{1}{e^{(E-\mu)/k_B T} + 1}$$

(E = energy; μ = → chemical potential). In the limit $(E - \mu) >> k_B T$ the Fermi-Dirac distribution approaches the → Boltzmann distribution. In the case of fermions, the chemical potential μ is also referred to as the Fermi energy ε_F ($\mu \equiv \varepsilon_F$).

Fermi Energy ε_F: reference energy of the → Fermi distribution describing the occupation of the states with low energy and how with increasing energy the states become unoccupied. In the limit of zero temperature all states below ε_F are occupied and above ε_F unoccupied.

Fermi Surface: (2-dimensional) surface in (3-dimensional) → **k**-space separating the occupied states at low energies from the unoccupied states at high energies. A sharp Fermi surface in **k**-space results if the number of particles and, hence, the → Fermi energy in the system are large and the temperature is low.

Ferromagnetism: caused by the spontaneous parallel orientation of the spin magnetic moments of the atoms or molecules in a crystal.

Flux-Flow Resistance: electrical resistance in a superconductor caused by the motion of magnetic flux lines (vortices).

Flux Pinning: disruption of the motion of magnetic flux lines in a superconductor effected by local inhomogeneities in the material, where the flux lines become trapped.

Free-Electron Aproximation: treating the electrons in a crystal as nearly free particles experiencing only a weak perturbation due to the (small) periodic potential of the crystal lattice.

Fullerenes: carbon molecules with an all-round completely closed structure consisting of various specific numbers of carbon atoms.

Giant Magnetoresistance: appears in the form of an extremely sensitive magnetic-field dependence of the electric resistance of specific multilayer structures of ferromagnetic layers.

Grain Boundary: location in a crystalline material, which separates individual single-crystalline grains with a different crystal orientation.

Hall Effect: electric voltage (Hall voltage) generated by the electric current flow in a magnetic field due to the → Lorentz force acting upon the charge carriers. The Hall voltage is directed perpendicular to both the direction of the current flow and the direction of the magnetic field.

Hooke's Law: proportionality between the elastic strain of a material and the mechanical load, named after the Englishman Robert Hooke.

Inelastic Scattering: a scattering process for which the energy of the incoming and the outgoing wave (neutrons, X-rays, etc.) differs due to an energy transfer between the wave and the scattering object.

Interference: superposition of two or more propagating waves, resulting in a spatial pattern of locations where the wave amplitudes add to or subtract from each other.

Josephson Effect: occurs at the weak contact between two superconductors in the form of voltage oscillations at high frequencies during electric current flow above a critical value of the current. The Josephson contact represents the device displaying a fundamental relation between voltage and frequency underlying the "Josephson voltage standard".

Kelvin: unit of the absolute temperature scale. Zero Kelvin corresponds to minus 273.15 °Celsius.

k- Space or Wave-Vector Space: mathematical space taken up by the → wave vectors **k**. This geometric concept is helpful for discussing the properties of many-body systems such as electrons in crystals (→ Fermi surface).

Landau Cylinder: cylindrical region in $\rightarrow$ **k**-space occupied by the electrons in a crystal, resulting from the energy quantization $h\nu_C$ for the electrons in a magnetic field. h is Planck's constant and ν_C the cyclotron frequency. In the case of two-dimensional systems ($\rightarrow$ two-dimensional electron gas) the Landau cylinders are reduced to Landau circles.

Lorentz Force: experienced by an electric charge moving in a magnetic field. The force is directed perpendicular to both the direction of the motion and the direction of the magnetic field.

Magnetic Flux Quantum: quantized unit of the magnetic flux (magnetic field $\times$ enclosed area) passing through the area. In a $\rightarrow$ two-dimensional electron gas the magnetic flux quantum is h/e, in the case of a superconductor it is h/2e .

Magnetic Penetration Depth of a Superconductor: small distance by which a magnetic field penetrates into a superconductor beyond its surface (before the field is completely compensated by the electric shielding current).

Magneto-Resistance: increment of the electric resistance due to the presence of a magnetic field.

Magnon: energy quantum of a $\rightarrow$ spin wave.

Meissner Effect: (or Meissner-Ochsenfeld effect) expulsion of a magnetic field from the interior of a superconductor. It is effected by electric shielding currents flowing along the surface of the superconductor within a thin layer having a thickness given by the $\rightarrow$ magnetic penetration depth. It is named after Walther Meissner and Robert Ochsenfeld, who discovered it.

Metal Fatigue: weakening of the mechanical strength of a material due to (in particular cyclical) mechanical loads. It starts with hardly visible microcracks, which subsequently grow larger and larger until the material breaks.

Micrometer: length unit of 10^{-6} meter.

Nanometer: length unit of 10^{-9} meter.

Nuclear Magnetism: spatial ordering of the magnetic moments associated with the nuclei.

Pancake Vortex: appears in form of a disk containing a $\rightarrow$ magnetic flux quantum in a highly anisotropic superconductor, where the superconductivity originates in distinct crystallographic planes (for example, the copper-oxide planes in the cuprate high-temperature superconductors) and where the magnetic field is oriented perpendicular to the planes.

Paramagnetism: caused by the spatial orientation of the intrinsic angular momentum or spin of the electrons along the direction of an applied magnetic field.

Pauli Exclusion Principle: it applies to systems obeying the → Fermi-Dirac statistics and states that each quantum mechanical state can be occupied at most only by a single particle.

Phonon: energy quantum $E = h\nu$ of a vibrational mode with the frequency ν of the lattice atoms in a crystal. h is Planck's constant $h = 6.626 \cdot 10^{-34}$ J s .

Photoelectric Effect: emission of electrons from a metal surface irradiated with light or more generally with electromagnetic waves. Whereas the energy of the emitted electrons is determined by the frequency of the radiation, the number of the electrons is given only by the intensity of the radiation.

Photon: energy quantum $E = h\nu$ of an electromagnetic wave with the frequency ν. h is Planck's constant $h = 6.626 \cdot 10^{-34}$ J s .

Planck's Radiation Law: describes the spectral energy distribution of the electromagnetic waves within a cavity under equilibrium at temperature T (→ Bose-Einstein distribution of the photons).

Quantized Electric Conductance: in a narrow one-dimensional channel (quantum wire) the → ballistic propagation of electrons is quantized in units of $2e^2 / h$.

Quantum Dot: artificial object being so small in all of its dimensions (quasi zero-dimensional) such that the quantum mechanical wave function of the electrons is dominated by its spatial size (like in an atom, why quantum dots are also referred to as "artificial atoms").

Quantum Statistics: applies to elementary particles which cannot be distinguished from each other. Depending on the angular momentum of the particles, one distinguishes between → Bose-Einstein and → Fermi-Dirac statistics.

Radiation Damage: structural changes in a material effected by its exposure to radiation (electromagnetic waves, particles).

Specific Heat: change of the internal energy associated with the change in temperature.

Spin Wave: energetic excitation of the spin magnetic moments in a spin lattice resulting in a deviation from the exactly parallel (in the case of a ferromagnet) or antiparallel (in the case of an antiferromagnet) orientation of neighboring spin magnetic moments.

Squid: Superconducting **Q**uantum **I**nterference **D**evice. It consists of a small superconducting loop interrupted by Josephson contacts. It represents the most sensitive device for measuring magnetic fields.

Superlattice: artificial structure in which two different metals or semiconductors are alternately stacked on top of each other with atomic regularity.

Symmetry: characterizes an arrangement of objects (for example, atoms or molecules in a crystal), the arrangement being exactly reproduced following certain (symmetry) operations such as translation, rotation, or mirror reflection.

Synchrotron Radiation: electromagnetic radiation emitted from electrons circulating at high velocities within an evacuated annular ring.

Tunnel Junction: a device in which two electrically conducting electrodes are separated from each other by an extremely thin insulating layer, such that electric current flow through the junction is only possible by means of the quantum mechanical tunneling process of the charge carriers.

Two-dimensional Electron Gas: electrically conducting layer at the surface of a semiconductor or at the interface between two semiconductors.

Type-I and Type-II Superconductor: classification according to the difference between the $\rightarrow$ magnetic penetration depth and the $\rightarrow$ coherence length.

Valence Band: completely filled $\rightarrow$ energy band below the $\rightarrow$ conduction band.

Wave Vektor: the inverse of the wavelength λ multiplied by 2π is defined as the wave number $k = 2\pi / \lambda$. In 3-dimensional space the direction of a propagating wave is described by the wave vector $\mathbf{k} = \mathbf{k}_x + \mathbf{k}_y + \mathbf{k}_z$, having the 3 components $\mathbf{k}_x$, $\mathbf{k}_y$, and $\mathbf{k}_z$ along the directions of the 3 coordinate axes, respectively.

Weiss Field: an effective magnetic field existing in a ferromagnetic material and postulated by Pierre Weiss for explaining phenomenologically $\rightarrow$ ferromagnetism.